Climate Change, Deforestation, and the Expansion of the Global Agricultural Frontier

Allan Hsiao
Stanford

Jacob Moscona
MIT

Benjamin A. Olken
MIT

Karthik A. Sastry
Princeton

January 20, 2026

Abstract

This paper studies how global warming affects deforestation and agricultural land use. Using global, high-resolution data on temperature, deforestation, and land cover from 2001 to 2019, we find that extreme heat causes large and persistent forest loss on the world's agricultural frontier. This effect is strongest in the tropics, in areas with the most temperature-sensitive crops, and in regions with the most inelastic demand for agricultural products, and we find no evidence that it is offset by global spillovers. Deforestation in response to extreme heat can be explained almost entirely by cropland expansion. We corroborate these findings using agricultural census data from Brazil, where extreme heat leads to productivity declines, cropland expansion, and limited additional input adjustment or land reallocation. Our estimates imply that extreme heat has already driven substantial forest loss and that projected warming through 2100 could lead to an additional 28 million hectares of deforestation. These findings challenge the view that economic reallocation will necessarily soften the economic and environmental consequences of climate change, suggesting instead that farmers double down and expand cropland locally in response to lower productivity.

Acknowledgments: We are grateful to Juliano Assunção, Chris Barrett, Francisco Costa, John Grigsby, Ishan Nath, Richard Rogerson, and seminar participants at Princeton University, the University of Michigan, the Coase Project, and the 2025 LACEA Annual Meeting (Recife) for helpful comments. We thank Bingqing Yang and Luong Nguyen for truly outstanding research assistance. All errors are our own.

1 Introduction

Rising temperatures have dramatically affected agricultural productivity around the world (Lobell and Field, 2007; Schlenker and Roberts, 2009; Lobell et al., 2011; Hultgren et al., 2025). How does this phenomenon affect global deforestation and agricultural land use?

There are two competing hypotheses regarding this relationship, each of which has starkly different implications. One hypothesis is that places where climate change harms agricultural productivity devote less land to agriculture while places where climate change improves agricultural productivity (in relative terms) devote more (e.g., Costinot et al., 2016). This strong realignment of economic activity in response to evolving comparative advantage is a natural outcome if global barriers to re-specialization, factor mobility, and trade are low (e.g., Cruz and Rossi-Hansberg, 2024). The resulting reallocation could potentially mitigate substantial damages to both agricultural productivity and the environment (e.g., Davis et al., 2017; Rising and Devineni, 2020; Beyer et al., 2022).

A second hypothesis, however, is that agricultural land use actually expands in areas that become less productive. This prediction is closely related to Norman Borlaug's classic hypothesis that the expansion of unproductive agriculture onto new lands is a principal driver of deforestation (Borlaug, 2000), as well as the observation that agriculturally unproductive parts of the world must be particularly agriculturally intensive in order to meet local subsistence needs (Schultz, 1953; Gollin et al., 2007; Nath, 2025). Expansion in unproductive places is a natural outcome if agricultural products are produced and consumed locally, and therefore farmers react to productivity losses by cutting down forests to expand land under cultivation. By implication, climate change could further entrench agricultural production and exacerbate environmental harm in affected locations.

This paper empirically investigates the relationship between global warming, deforestation, and agricultural land use at the global scale. Using gridded data at the one-degree grid-cell level, we find that increased exposure to extreme heat causes local deforestation. This effect is persistent and not mitigated by spatial spillovers. Consistent with the view of agricultural "entrenchment," extreme heat drives local cropland expansion, and the link between heat and deforestation is strongest in places that face relatively inelastic agricultural demand and grow relatively heat-intolerant crops. Quantitatively, extreme heat exposure from 2015 to 2019 led to 1.4 million hectares of forest loss, driven by deforestation in tropical countries and especially by deforestation in Brazil. Projected temperature increases could lead to 28 million hectares of additional forest loss by 2100, equivalent to 26% of all deforestation and 48% of tropical deforestation observed in sample.

Model. To fix ideas, we begin our analysis with a simple model of agricultural production and deforestation. Farmers produce agricultural output using land. They take as given local agricultural productivity, local costs of clearing land, and the shadow price of agricultural output. The last is determined by an equilibrium process that we keep flexible. We allow, for example, the extent of market integration to vary by place and for farmers to face constraints (e.g., subsistence requirements or credit constraints), such that private valuations do not coincide with market prices.

An extreme heat shock affects incentives to deforest through three channels: productivity, prices, and costs. Lower productivity reduces the incentive to clear land. By contrast, higher prices and lower costs of clearing the forest increase the incentive to clear land. The net effect is ambiguous and depends on the relative strength of the three channels. That is, extreme heat can lead to more deforestation, which we call the "entrenchment" case, or less deforestation, which we call the "reallocation" case. Furthermore, extreme heat has *indirect* effects through agricultural prices, which will always lead to (weakly) more deforestation in regions that are not directly affected by the shock. This theoretical ambiguity motivates our empirical analysis, which investigates these forces directly.

Data and Measurement. We first compile data on deforestation in each year since 2000 from Hansen et al. (2013). We complement these data with an alternative measure of deforestation that relies on land cover data from the European Space Agency (ESA) (Zanaga et al., 2021). We also obtain an independent measure of area cleared by fires (Chen et al., 2023), since fires are a common method to clear land for agricultural production in poor countries with particularly pronounced effects on carbon emissions (Page et al., 2002).

We use the ESA land cover data to measure agricultural land use at a global scale. We obtain more precise measures of land use in an important deforestation hotspot from the latest three rounds of the Brazilian Agricultural Census (1996, 2006, 2017). To proxy for short-run fluctuations in agricultural productivity, we compile global data on the Normalized Difference Vegetation Index (NDVI), a satellite-based indicator of plant health commonly used to proxy for agricultural output.

Finally, we measure daily temperature realizations using the ERA-5-Land database from the European Centre for Medium-Range Weather Forecasts (Muñoz Sabater et al., 2021). Motivated by existing work documenting that extreme heat exposure is the main channel through which the weather affects agricultural productivity (e.g., Schlenker and Roberts, 2009; Hultgren et al., 2025), we construct a negative productivity shock in each grid cell and year as the number of "killing degree days": the time exposure to temperatures above 32°C, weighted by their distance from the threshold.

We conduct our main analysis at the level of one-degree grid cells, which are 110 km

wide at the equator. This choice allows us to focus on "local" environmental and economic outcomes in a uniform way throughout the world. In robustness checks, we show the stability of our conclusions to different choices for geographic units.

We focus much of our analysis on the "Global Arc of Deforestation." We define this by first designating areas with more than 50% forest cover as "forest," and then defining grid cells on the border between forest and non-forest as the Arc.[1] Our hypothesis is that the effect of temperature change on deforestation—regardless of its sign—is strongest in the Arc, where most marginal, undeveloped land is initially forested. The Arc is the active frontier of agricultural expansion.

Main Results. Our main estimating equation captures the effect of changes in killing degree days on deforestation at the level of 1° by 1° grid cells and years. The regression model includes grid-cell and country-by-time fixed effects. The former absorb place-specific linear trends.[2] The latter absorb both global trends and changes in country-specific regulation or enforcement (e.g., Burgess et al., 2024). Causal identification relies on the randomness of local temperature extremes, conditional on these fixed effects.

Our main finding is that extreme temperatures cause local deforestation. This effect persists for several years following the shock, and the long-run effect summed over five years is an order of magnitude larger than the contemporaneous effect. The lack of a dynamic "sign reversal" establishes that extreme heat exposure in a given year has permanent effects on forest cover, and rules out the alternative possibility that deforestation is merely re-timed. We moreover find no evidence of pre-existing trends, suggesting no role for reverse causality (e.g., if deforestation in the past raises temperatures today) or anticipation. The baseline effect is more than twice as large in the tropics compared to the non-tropics. When we turn to quantification, this difference in magnitude—combined with the fact that the tropics also have greater exposure to extreme heat—will imply that climate change has a disproportionate effect on deforestation in the tropics, precisely where forest loss is most environmentally harmful.

The main result that temperature extremes induce deforestation is robust to a number of alternative specifications. These include the use of alternative measures of deforestation, alternative definitions of the Arc of Deforestation, alternative temperature thresholds to measure killing degree days, and models that include a range of additional controls, in-

[1] Our categorization generalizes the notion of the "Arc of Deforestation" that exists in studies of the Brazilian Amazon (e.g., Fearnside, 2005; Csillik et al., 2024), where most deforestation occurs in areas between the deep Amazon and agricultural lands.

[2] Failing to account for these location-specific trends can lead to spurious inference about the effects of temperature extremes on outcomes. Since our regression is in first-differences, location fixed effects are akin to including location-specific time trends in a linear model, as suggested by Jones et al. (2025).

cluding place-specific linear "accelerations" (i.e., linear trends in a first-differences model) and measures of upwind exposure to deforestation (Araujo et al., 2023). We also show that extreme heat exposure is associated with greater fire setting, a specific form of land clearing that is common in developing countries and which has independent negative effects on both local health and carbon emissions (Page et al., 2002).

We find no evidence that local deforestation is mitigated by spillovers across regions. To test for these spillovers, we construct a location-specific measure of shocks in other parts of the world that grow the same crops, proxying for exposure to global price changes. Augmenting our baseline model with this measure, we are able to capture spillovers through prices while maintaining our model specification that controls for time fixed effects and thus leverage the same identifying variation as our baseline specification. The null spillover effects rule out the possibility that increased deforestation in heat-affected areas is offset by decreased deforestation elsewhere. Instead, the local effects we uncover seem to add one-for-one to the global tally of deforestation.

Mechanisms. We next study the mechanisms by which extreme heat induces deforestation. Our main hypothesis is that lower agricultural productivity incentivizes cropland expansion, especially in settings where food demand is particularly inelastic.

First, we show that the extreme heat shocks that we measure induce substantial and immediate declines in NDVI, suggestive of a negative effect on agricultural productivity. We find no effects of extreme temperatures on NDVI in the deep forest far from the Arc of Deforestation, suggesting that the decline in NDVI is primarily picking up declining crop productivity rather than declining tree health.

Second, we show that the effect of extreme heat on deforestation is largest in regions that cultivate heat-sensitive crops, for which killing degree days have the largest effect on agricultural productivity. To measure local crop sensitivity, we combine data from EarthStat on the crop composition of each grid cell in 2000 (Ramankutty et al., 2008) with data on crop-specific temperature sensitivity from the Food and Agriculture Organization's EcoCrop Database in order to calculate the average temperature sensitivity of crops grown in each grid cell (see Moscona and Sastry, 2023; Hsiao et al., 2025). This finding further supports the hypothesis that deforestation is a result of lower local productivity.

Third, we show that the effect of extreme heat on deforestation is largest in regions with the most inelastic food demand. To measure this, we compile data on crop-by-region elasticity estimates from the USDA Commodity and Food Elasticities database and, combining these estimates with crop composition data from EarthStat, calculate the average local demand elasticity of the crops grown in each grid cell. This finding is consistent with the hypothesis, illustrated in the model, that price effects drive deforestation: that is,

adverse shocks raise incentives to deforest by significantly increasing local food prices. We also find larger effects of heat on deforestation when we estimate our baseline specification on larger geographic units (five-by-five degree cells), which are plausibly less integrated with one another than the one-by-one degree cells that comprise our baseline sample.

Fourth, we show direct evidence that extreme heat shocks lead to cropland expansion. Using a satellite-derived measure of land devoted to crop cultivation in each cell and year from the ESA, we find that extreme heat shocks lead to cropland expansion that accumulates over several years. While changes in cropland are more challenging to detect from satellite imagery than changes in forested area, the estimates imply that cropland expansion can explain nearly all of the forest loss to deforestation. Like deforestation, cropland expansion is concentrated in the tropics and does not take place far away from forested areas, where opportunities to clear new land are more limited.

Finally, we use census data from Brazil to study how temperature shocks affect land use and input changes in greater detail. Combining the 1996, 2006, and 2017 rounds of Brazil's Agricultural Census, we find that municipality-level extreme heat exposure leads to cropland expansion during the subsequent decade. We find no evidence of pasture land expansions or of increased labor use, suggesting that extreme heat represents a negative shock that is specific to cropland productivity, which in turn drives deforestation through the channels discussed above. Despite the expansion of agricultural land use, extreme heat exposure nevertheless reduces agricultural output and substantially lowers agricultural output per area, driven both by lower productivity on existing land and the fact that production expands to *ex ante* less productive areas. Thus, rather than shifting away from the most heat-exposed regions, these estimates further emphasize that cropland expands in exactly the regions that are most exposed to damaging temperatures.

Quantification. We combine our baseline estimates with data on extreme heat exposure from the sample period and projections of extreme heat exposure through the end of the century in order to quantify the aggregate effect of rising temperatures on past and future deforestation. From 2006 to 2019, we estimate that extreme heat exposure led to 1.42 million hectares of forest loss, or over one thousand square kilometers per year. This is largely driven by tropical deforestation, and especially by Brazil, where heat-induced deforestation can explain over 8% of all deforestation during the period. By the end of the century, under a "middle of the road" climate scenario (SSP 2-4.5), our estimates imply that extreme heat will cause an additional 30 million hectares of tropical deforestation, an area larger than Italy, the Philippines, or Arizona. This would represent a substantial increase compared to past deforestation trends. For example, predicted heat-induced tropical deforestation amounts to 48% of all tropical deforestation and 134% of Brazilian

deforestation that has taken place from 2005 to 2019. Under a much more extreme, but still possible, climate scenario (SSP 5-8.5), these figures jump to 152% and 394%, respectively.

Related Literature. Our paper relates to several strands of literature. First, we contribute to work on the economics of deforestation, including recent empirical studies of deforestation in tropical regions (e.g., Assunção et al., 2015, 2023; Burgess et al., 2012, 2024, 2025; Akerman, 2025).[3] Our focus on the impact of changing agricultural productivity is related to microeconomic studies that investigate how agricultural input, technology, or price shocks affect local deforestation (Barrett, 1999; Pelletier et al., 2020; Abman et al., 2020; Abman and Carney, 2020; Carreira et al., 2024; Szerman et al., 2024). Our analysis of spillover effects and interpretation of the Borlaug hypothesis relates our work to Farrokhi et al. (2025), who study how changes in trade costs affect global deforestation.

Second, we connect to studies of land and labor reallocation in global agriculture (e.g., Hertel, 2002, 2013; Gollin et al., 2007; Moscona and Sastry, 2025; Carleton et al., 2025; Farrokhi et al., 2025). Our findings are consistent with the argument in Nath (2025) that trade frictions limit sectoral reallocation in response to climate change. This in turn harkens back to the theoretical analysis of Matsuyama (1992) showing that agricultural productivity improvements can lead to growth or shrinkage of the agricultural sector depending on openness to trade. We resolve this theoretical ambiguity by directly estimating how temperature shocks affect land use and deforestation.

Finally, we build on a large body of work studying climate impacts and adaptation. Unlike much of the existing empirical literature on agricultural damages (e.g., Lobell and Field, 2007; Schlenker and Roberts, 2009; Lobell et al., 2011; Burke and Emerick, 2016; Moscona and Sastry, 2023; Hsiao et al., 2025; Hultgren et al., 2025), we focus on the margin of land use and its environmental footprint. This focus is shared by quantitative analyses of spatial reallocation in agriculture (e.g., Costinot et al., 2016) and of multi-sector spatial integrated assessment models (e.g., Cruz and Rossi-Hansberg, 2024). Our empirical results pose a challenge for quantitative analyses that predict decreased agricultural investment in the tropics as global warming accelerates. For such models, our empirical estimates are informative about the direction and magnitude of local land use changes, as well as the mechanisms that shape adaptation to climate shocks.

[3] See Balboni et al. (2023) and Costa et al. (2025) for recent surveys. Hsiao (2025), Barrozo (2025), and Mishra (2025) perform related quantitative analysis of deforestation across space.

2 Model

To fix ideas, we present a simple model of agricultural production, land use, and deforestation. Due to competing forces, extreme temperature exposure could lead to either increased or decreased deforestation. This formalizes versions of both contrasting hypotheses described in the Introduction and motivates our empirical analysis. We focus on a single period model here to fix the core ideas; we discuss dynamics below and in more detail in Appendix B.

Set-up. The world consists of locations indexed by $i \in \mathcal{I}$. In each location, farms produce using x_i units of land. They have productivity a_i and they produce output with a (shadow) price p_i. We take the flexible interpretation that p_i could incorporate the value of easing subsistence or financial constraints, and therefore remains defined even in places without functioning agricultural markets. To obtain x units of land, farmers must clear the forest at cost $-\frac{c_i}{2}x^2$, where $c_i > 0$ is a local cost shifter. Thus, farmers' land use decision in each location is described by the profit maximization problem

$$x_i \in \arg\max_{x>0} \left\{ p_i a_i x - \frac{c_i}{2} x^2 \right\}, \qquad \forall i \in \mathcal{I} \tag{1}$$

taking p_i, a_i, and c_i as given. We let $q_i = a_i x_i$ denote realized agricultural output. Local prices are determined by the system of equations

$$p_i = P_i\left((q_j)_{j \in \mathcal{I}} \right), \qquad \forall i \in \mathcal{I} \tag{2}$$

where we assume that each function P_i, which is potentially location-specific, is decreasing in all arguments. That is, food scarcity weakly increases prices. This formulation allows us to capture a number of possible market structures, such as those more or less open to cross-location trade. An equilibrium is a vector of land-use decisions and prices such that farmers optimize (equation 1) and markets clear (equation 2), given fundamentals $(a_i, c_i)_{i \in \mathcal{I}}$.

Implications for Local Deforestation. Each farmer i's optimal land-use choice, derived from the first-order condition of equation (1), is $x_i = p_i a_i / c_i$. We interpret local extreme temperature exposure as a shifter of the exogenous parameters a_i and c_i, which in turn can affect the endogenous price p_i. As such, the effect on deforestation in location i is

$$\Delta \log x_i = \Delta \log a_i + \Delta \log p_i - \Delta \log c_i \tag{3}$$

This equation embodies three forces that shape the pathway from extreme temperatures to deforestation. First, there is a productivity effect ($\Delta \log a_i$): farmers want to use more land if it is more productive. Second, there is a price effect ($\Delta \log p_i$): farmers want to use more land if the price of food increases. Third, there is a cost effect ($-\Delta \log c_i$): farmers want to use less land if the cost of clearing the forest increases.

Depending on the relative size of these three channels, a climate shock to local fundamentals could either decrease or increase local deforestation. One possibility is that rising temperatures reduce productivity net of opportunity costs, $\log a_i - \log c_i$, more than they increase local prices, $\log p_i$. In this "reallocation" case, temperature shocks lead localities to deforest less and allocate less land to agriculture ($\Delta \log x_i < 0$). Alternatively, rising temperatures might reduce productivity net of opportunity costs less than they increase local prices. In this "entrenchment" case (the Borlaug Hypothesis), temperature shocks lead localities to deforest more and expand land devoted to agriculture ($\Delta \log x_i > 0$).

An illustrative calculation that nests both cases can be obtained when agricultural markets are fully localized with elasticity of demand δ_i: $\log q_i = -\delta_i \log p_i$. Plugging this demand curve into equation (3) and simplifying yields

$$\Delta \log x_i = \frac{\delta_i - 1}{\delta_i + 1} \Delta \log a_i - \frac{\delta_i}{1 + \delta_i} \Delta \log c_i \tag{4}$$

For sufficiently inelastic demand ($\delta_i < 1$), $\Delta \log x_i$ decreases in $\Delta \log a_i$: that is, despite the productivity effect, the increase in prices is sufficient for lower productivity to induce deforestation, even holding fixed costs. When $\delta_i \to 0$, $\Delta \log x_i = -\Delta \log a_i$: the change in land use must exactly offset the loss in productivity to achieve the same amount of food production. This is the basic logic of the "food problem" described by Schultz (1953).

Implications for Global Spillovers. Different locations interact in the simple model through output prices. Thus, in location $j \neq i$, the response to an i-specific shock occurs only through the price channel: $\Delta \log x_j = \Delta \log p_j$. If agricultural production declines in location i, and prices everywhere are weakly decreasing in quantities in any location, then this price effect is positive: $\Delta \log x_j > 0$. Thus, leakage or "spillovers" always manifest as additional deforestation in indirectly affected locations. These effects scale with the extent of price effects, so we would expect them to be larger if, for example, markets in i and j are more integrated with one another: for example, if they grow the same crops.

Dynamics. In Appendix B, we augment this simple model to explicitly consider dynamics with adjustment costs. A new prediction is that deforestation occurs slowly in response to shocks. Thus, to account for the full effects of a given shock on deforestation it

is necessary to consider the full time path of responses, motivating the inclusion of lagged effects in our main empirical model.

The Road Ahead. This simple model conveys that local extreme heat can either increase or decrease local deforestation. Moreover, the sign and magnitude of this effect is governed by the extent of local productivity effects and the extent of local price movements. Global spillovers can amplify the effects of adverse shocks on total global deforestation, and they scale with price effects that link locations through output markets. And, dynamically, the full effects of extreme heat on land use can take time to unfold. These predictions will motivate our main empirical analysis and our investigation of mechanisms.

3 Data and Measurement

3.1 Deforestation and Land Use

Forest Loss. We measure deforestation using the global forest change data set originally introduced by Hansen et al. (2013). The data are originally constructed by using Landsat satellite images at a 30-meter resolution since 2000 to determine whether each pixel was deforested in each year. Combined with data on the percent tree cover of each pixel p in 2000, also reported by Hansen et al. (2013), we use this information to construct our main measure of deforestation at the level of one-by-one-degree grid cells and years:

$$\text{Deforestation}_{it} = \frac{100}{\text{Area}_i} \cdot \sum_{p \in i} \mathbb{I}_{\text{Loss Year}_p = t} \times (\text{PctForestCover}_{p,2000} \cdot \text{Area}_p) \tag{5}$$

where $\mathbb{I}_{\text{Loss Year}_p = t}$ is an indicator if forest cover in pixel p was lost in year t; $\text{PctForestCover}_{p,2000}$ is the percent forest cover of pixel p in 2000; and Area_i and Area_p are the areas of cell i and pixel p respectively. This measure captures forest loss as the percent of grid cell i (0-100) that was deforested in year t.

This is the main measure of deforestation used in our empirical analysis. In sensitivity analysis, we also use a measure of deforestation produced by the European Space Agency (ESA), measured in the same units (Zanaga et al., 2021). While the Hansen et al. (2013) data are based on Landsat imagery, the ESA data rely on independent analysis of satellite imagery from the Sentinel and Copernicus programs. This makes it useful for validation of our main results.

Fires. Fire setting is a common strategy used for forest clearing, especially in tropical regions. We use data from the Global Fire Emissions Database (GFED) to measure the

share of each grid cell that was burned in a fire in each year (Chen et al., 2023). These data were constructed using Moderate Resolution Imaging Spectroradiometer (MODIS) satellite imagery and, in that sense, provide independent information relative to both measures of deforestation described above.

Agricultural Land Use. We use two different approaches to measure agricultural land use. First, we use the aforementioned land cover data from the ESA to measure cropland in each grid cell and year. This is our main measure of agricultural land use in the global sample of grid cells.

Second, we use data from the last three rounds (1996, 2006, and 2017) of the Brazilian Agricultural Census to measure changes in agricultural land use across Brazilian municipalities. The Census is constructed from detailed interviews with farmers conducted roughly once per decade and, in contrast to the satellite data, represents an on-the-ground assessment of agricultural expansion.

Lastly, as a proxy for local plant health, we compile global data on the Normalized Difference Vegetation Index (NDVI), a widely used, satellite-based indicator of the presence and health of plant cover. These data are constructed by NASA's Earth Observing System using MODIS satellites and reported at the 0.1 degree level in each month.

3.2 Extreme Heat Exposure

We measure historical temperatures using the ERA5-Land database from the European Centre for Medium-Range Weather Forecasts (Muñoz Sabater et al., 2021). This reanalysis dataset combines weather observations from around the world with a model to generate gridded (0.25-by-0.25 degrees), hour-by-hour temperature measurements. We compile all data since 2000 and aggregate observations to the one-by-one degree grid-cell level.

We use these data to measure exposure to killing degree days in each grid cell i and year t:

$$\text{KDD}_{it} = \sum_{s=T^{\text{kill}}}^{\infty} \frac{\text{hours}(s, s+1)}{24} \left(s + \frac{1}{2} - T^{\text{kill}} \right) \tag{6}$$

where s sums over temperature increments, $\text{hours}(s, s+1)$ measures the number of hours spent between s° C and $s+1^\circ$ C, and T^{kill} is the temperature above which agricultural productivity begins to decline.[4] In words, KDD_{it} captures the number of fractional degree days in excess of T^{kill}. As our baseline, we set $T^{\text{kill}} = 32^\circ$ C, but we show results using different temperature thresholds.

[4] In practice, the data on temperature exposure are top-coded at 45 C. We treat all hours in excess of 45 C as having the temperature 45.5 C.

Figure 1: The Global Arc of Deforestation

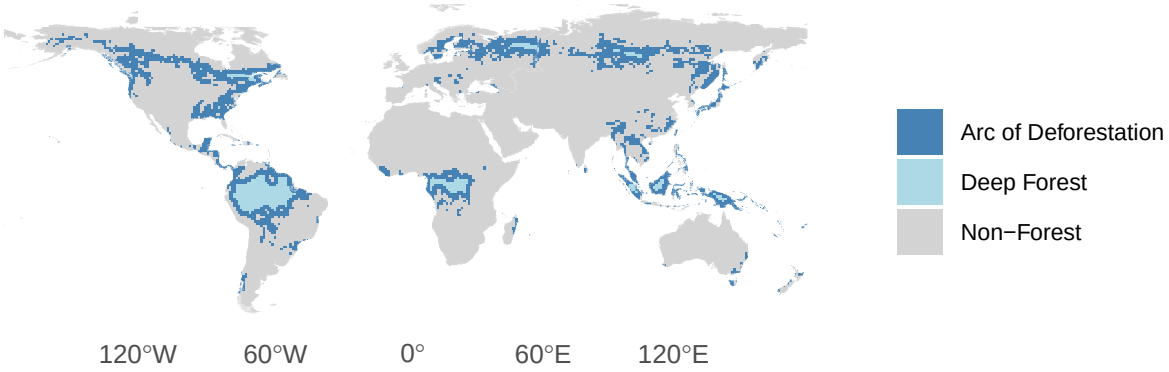

Notes: This figure shows our categorization of the world's forests at the start of our sample period in 2001. Each square is a one-by-one degree grid cell, our main unit of analysis. Squares colored gray ("Non-Forest") have less than 50% tree canopy cover according to the measure of Hansen et al. (2013), and squares colored blue (dark or light) have more. We partition this latter category into the Arc of Deforestation (dark blue) and Deep Forest (light blue) based on distance to the Non-Forest, as described in the main text.

Prior work has documented that extreme heat exposure—and, in particular, killing degree days (KDDs) in excess of particular temperature thresholds—is the main mechanism through which temperature affects agricultural productivity (Schlenker and Roberts, 2009; Butler and Huybers, 2013; Hultgren et al., 2025). We validate this measurement strategy in our own context by showing that increases in KDD exposure at the grid cell level causes substantially declines in cropland NDVI, which measures plant health (Figure A.1), even in cropland that is far away from forested areas.

3.3 The Global Arc of Deforestation

The economic mechanisms by which temperature change affects deforestation via agricultural expansion are most plausible at the edge of major global forests. Far outside the forest edge, there is little forest to cut down or scope for expanding cropland onto forested area. Deep inside the forest, there is little agricultural production or scope for expansion.

Therefore, for most of our analysis, we focus our attention on the "Global Arc of Deforestation" at the edge of the world's forests. To define this concept, we first define major global forests as all grid cells with greater than 50 percent forest cover in any given year. We then denote the forested area within two grid cells (i.e., within 2 degrees, or about 220 km at the equator) of any global forest border as the Arc of Deforestation. We refer to the remaining forested area as the *deep forest*.

Figure 1 displays the categorization of all grid cells at the start of our sample period in

2001. The Arc of Deforestation is displayed in dark blue and the deep forest is displayed in lighter blue. The edges of the world's major tropical forests, including the Amazon and Congolian Rainforests, are clearly visible in dark blue, in addition to many tropical forests in Southeast Asia and boreal forests in Canada, Russia, and Northern Europe.

While the Arc of Deforestation displayed in Figure 1 is our main definition, we also explore sensitivity to changing the threshold for defining a cell as the forest (i.e., using 30 or 80 percent forest cover instead of 50) and fixing the Arc of Deforestation at the start or end of the period instead of allowing it to change dynamically as forest cover evolves. We also show that our results are qualitatively similar if we use all forested grid cells as the regression sample instead of restricting attention only to the Arc of Deforestation.

4 Main Results

We now present our main results regarding the effect of temperature shocks on deforestation. We find that extreme heat exposure increases deforestation. The effect persists for several years, is larger in tropical regions, and is driven in part by fire setting.

4.1 Empirical Strategy

To take our motivating question to the data, consider equation (4), which states that the change in forest should be related to the change in productivity. The empirical analogue of equation (4) is our main regression specification:

$$\text{Deforestation}_{it} = \beta \, \Delta\text{KDD}_{it} + \gamma_i + \chi_{c(i),t} + \epsilon_{it} \tag{7}$$

where i indexes one-by-one degree grid cells, t indexes years, and $\text{Deforestation}_{it}$ and KDD_{it} are defined in Sections 3.1 and 3.2, respectively. γ_i and $\chi_{c(i),t}$ are fixed effects at the grid cell and country-by-year level. Standard errors are first-level administrative divisions, which typically correspond to states or provinces within countries.[5,6]

Our baseline model uses place- and year-specific variation in temperature extremes to isolate causal effects of temperature shocks while sweeping out possible confounds. The inclusion of place fixed effects absorbs, in this first-differences model, place specific linear trends.[7] The inclusion of country-by-time fixed effects allows us to absorb country-specific

[5] We assign grid cells to the country and sub-region that encompasses the largest share of their area.

[6] While our main specification is estimated in first differences, our baseline results are qualitatively and quantitatively similar when estimated in levels (Figure A.2, which mirrors Figure 2).

[7] Jones et al. (2025) show that failing to account for these trends can lead to spurious correlation between

(not just global) time trends in warming and deforestation. In particular, this allows us to capture any country-level changes in policy or policy enforcement, which have been shown to affect deforestation (Burgess et al., 2025), and isolate the effect of extreme heat fluctuations across cells within the same county.

The coefficient of interest is β. If $\beta > 0$, increases in extreme heat exposure lead to more deforestation. This would be consistent with the "entrenchment case" (or "Borlaug hypothesis"), in which higher (lower) agricultural productivity leads to less (more) deforestation. If $\beta < 0$, increases in extreme heat exposure lead to less deforestation. This would be consistent with the "reallocation case," which predicts the opposite relationships.

To study dynamics—which is important both to verify that there are no pre-existing trends and to capture the full effect of extreme heat on deforestation, which could take several years to accumulate—we estimate the following version of the model that includes leads and lags of the independent variable:

$$\text{Deforestation}_{it} = \sum_{j=-L}^{K} \beta_j \Delta\text{KDD}_{i,t-j} + \gamma_i + \chi_{c(i),t} + \epsilon_{it} \tag{8}$$

where the β_j are leads and lags of extreme heat exposure. When $j < 0$, the β_j capture pre-existing trends in the relationship between changes in extreme heat exposure and deforestation ("leads"); when $j > 0$, the β_j capture the extent of persistence in the effect of extreme heat shocks on deforestation ("lags"). Each coefficient represents the marginal effect of extreme temperature changes conditional on the changes in other years. When estimating the total effect of extreme heat on deforestation using (8), we also report $\sum_{j=0}^{K} \beta_j$, which captures the total effect of a permanent KDD shock at time t on deforestation from t through $t + K$.

4.2 Main Estimates: Extreme Heat and Deforestation

Figure 2 presents our baseline dynamic estimates from a version of equation (8) that includes the contemporaneous change, four leads, and four lags ($K = L = 4$). We find a positive and significant effect of extreme heat shocks on deforestation (dark blue estimates), both in a model with place and time fixed effects (Figure 2a) and in a model with place and country-by-time fixed effects (Figure 2b). The positive effect emerges in the year of the extreme heat shock and remains at a similar magnitude for the following two years, before declining in the third and fourth years after the shock. This finding rules out the hypothesis that deforestation is merely "re-timed" in response to changes as a form of

extreme temperature exposure and economic outcomes.

Figure 2: Extreme Heat Causes Deforestation

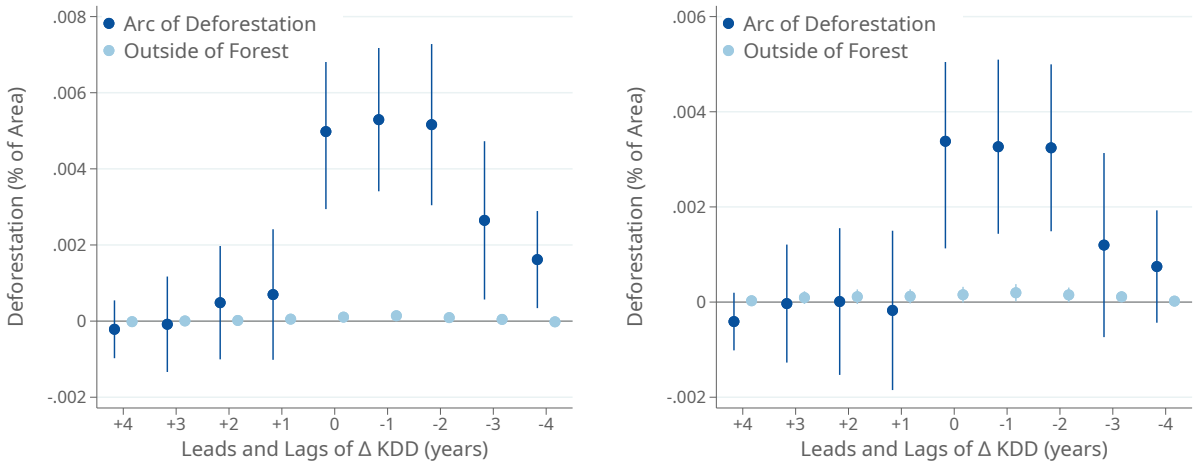

(a) Cell and Year Fixed Effects

(b) Cell and Country-Year Fixed Effects

Notes: This figure presents the dynamic effects of extreme heat exposure on deforestation. Each sub-figure reports estimate of equation (8) on two different samples: the Arc of Deforestation, in dark blue, and areas outside the forest, in light blue (see Section 3.3). In addition to the leads and lags of killing degree days, the estimates in Figure 2a include grid cell and year fixed effects and the estimates in Figure 2b include grid cell and country-by-year fixed effects. Error bars are 95% confidence intervals based on standard errors clustered by first-level administrative division (states within countries).

intertemporal substitution. Instead, changes have a permanent effect on forest cover that is neither mitigated nor reversed in the future. The dynamic model in Appendix Section B highlights how any convexity in the cost of deforestation generates this pattern in which the deforestation response to a persistent shock is spread over multiple years.[8]

All leading coefficient estimates are close to zero and statistically insignificant. This suggests that the main estimate is not driven by pre-existing trends that affect both extreme heat and deforestation and, moreover, rules out anticipation effects. There is no effect of extreme heat exposure on deforestation in non-forest area (light blue estimates), where opportunities for land expansion are likely more limited.

This result does not seem to be driven by units or choice of econometric specification. We obtain quantitatively and qualitatively similar estimates when the outcome and regressor are in levels rather than first differences (Figure A.2). We obtain the same sign and time pattern when using the logarithm of deforestation as the outcome (Figure A.3), indicating that extreme heat exposure leads to more deforestation not just in absolute but

[8]Killing degree day shocks do, in fact, have a persistent component; in particular, on average 20% of each shock to KDD remains in the following year and 18% remains after four years (Figure A.4). Thus, in expectation, a KDD_{it} shock in this year predicts higher killing degree days in future years.

Table 1: Extreme Heat Causes Deforestation: Cumulative Effect and Sample Splits

	(1)	(2)	(3)	(4)	(5)
		Arc of Deforestation			Non-Forest
	All	All	Tropics	Non-Tropics	All
	Panel A: Contemporaneous Effect				
ΔKDD	0.00196***	0.00253***	0.00331***	0.00033	-0.00001
	(0.00067)	(0.00071)	(0.00081)	(0.00059)	(0.00002)
Observations	45885	45587	19621	25966	230558
R-squared	0.448	0.513	0.591	0.400	0.424
	Panel B: Cumulative Effect				
Sum of ΔKDD	0.02534***	0.02331***	0.02634***	0.01083**	0.00018
	(0.00496)	(0.00538)	(0.00653)	(0.00419)	(0.00021)
Observations	48875	48564	20826	27738	243756
R-squared	0.430	0.497	0.575	0.383	0.413
Grid-Cell FE	Yes	Yes	Yes	Yes	Yes
Year FE	Yes	No	No	No	No
Country-Year FE	No	Yes	Yes	Yes	Yes

Notes: This table reports the effects of extreme temperature changes on deforestation. Panel A reports estimates of equation (7). Panel B reports estimates of equation (8) for j between $-L = 0$ and $K = 4$, where "Sum of ΔKDD" corresponds to the sum of coefficients: $\beta_0 + \beta_1 + \beta_2 + \beta_3 + \beta_4$. The set of included fixed effects is listed at the bottom of each column and the sample is noted at the top. The Tropics are defined as all grid cells that fall between the Tropic of Cancer and the Tropic of Capricorn, and the Non-Tropics as the complement. The Arc of Deforestation is defined in Section 3.3 to identify the edge of the world's forests, and the Non-Forest denotes grid cells with less than 50% tree cover. Standard errors, reported in parentheses, are clustered by first-level administrative division (states within countries).

also in relative terms.

Table 1 probes the precision and magnitude of these estimates in greater detail. Panel A reports estimates of equation (7), i.e., only the contemporaneous effect of extreme heat on deforestation. We find that $\beta > 0$ at a high degree of statistical significance, in a model with place and time fixed effects (column 1) and in a model with place and country-by-time fixed effects (column 2). The effect is much larger in magnitude for the tropics (column 3) than the non-tropics (column 4), where we define the tropics as the area between the Tropic of Cancer, $23.5°$ N, and the Tropic of Capricorn, $23.5°$ S. Again, there is no effect of extreme heat exposure on deforestation in non-forest area, as we define it (column 5).[9]

We next investigate the cumulative effect of an increase in extreme heat by estimating

[9]This is not mechanical; recall our definition of "non-forest" are 1 degree by 1 degree grid cells (i.e. about 110km by 110km at the equator) that are less than 50 percent forested, so it is possible there can be isolated pockets of forest even within these pixels that could be affected.

Figure 3: Long Difference (Decadal) Estimates

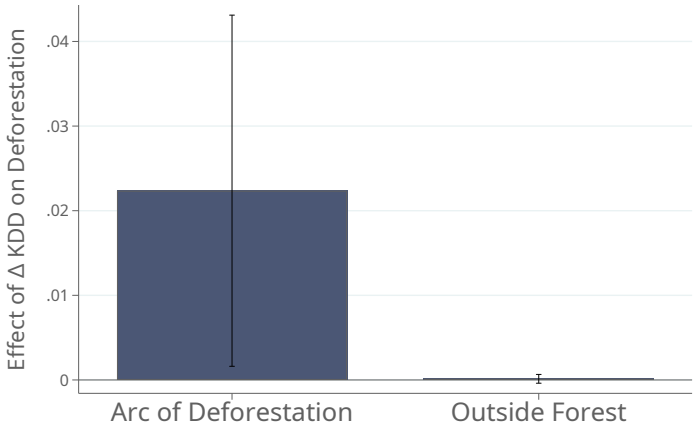

Notes: This figure reports long-difference estimates in which the unit of observation is a cell-decade pair. The Arc of Deforestation is defined in Section 3.3 to identify the edge of the world's forests, and the Non-Forest denotes grid cells with less than 50% tree cover. Grid cell and country-by-decade fixed effects are included. Error bars are 95% confidence intervals based on standard errors clustered by first administrative division (states within countries).

equation (8) with the contemporaneous effect, four lags ($K = 4$), and no leads ($L = 0$). Table 1, Panel B, reports the sum of the coefficients from this model. The sum of coefficients is roughly ten times the contemporaneous effect alone (column 1), again suggesting that effects build up substantially over time. The effect size is similar after isolating within-country variation by including country-year fixed effects (column 2). The cumulative effect remains larger in the tropics compared to the non-tropics (columns 3-4); but, unlike in the purely contemporaneous analysis (Panel A), we detect a positive and significant effect outside of the tropics as well.

Long-Difference Estimates. As an alternative strategy to capture the long-run effect of extreme heat on deforestation, we estimate a stacked long difference in which we aggregate both the right and left-hand sides of equation (7) to the decade level (2000s and 2010s) and estimate it as a two-decade panel with place and decade fixed effects. This estimating equation is equivalent to (7), except t indexes decades instead of years. We obtain a coefficient estimate that is very similar to the sum of the lagged effects in Panel B of Table 1 (Figure 3, bar 1). This is further evidence that the effect of extreme heat shocks on deforestation persists and is not undone by subsequent land use changes.[10] We continue

[10]We also find no evidence of pre-existing trends in the long-difference specification, though since we only have two decades, we use a different strategy to check for this since we cannot plot detailed event studies. In particular, we find no evidence that extreme heat in the 2010s is associated with deforestation in the 2000s (Figure A.5) i.e., deforestation in the current decade is uncorrelated with extreme heat exposure in

to find no evidence that extreme heat affects tree loss away from major forests (bar 2).

Alternative Measurement Strategies. We conduct a range of sensitivity analyses of the measurement approach in our baseline results. First, to make sure that the results are not driven by some specific feature of the Hansen et al. (2013) data, we present qualitatively similar results using independent deforestation data from the ESA (Table A.1).

Second, we show that the results are very similar using alternative definitions of the Arc of Deforestation (Table A.2). This includes defining forested grid cells as those with either 50% (baseline), 30%, or 80% forest cover (columns 1-3), as well as holding the arc constant throughout the sample period (columns 4 and 5). The results are also similar if we use different sized geographic units within the Arc of Deforestation (Table A.3).

Third, we show that the baseline results are very similar (albeit slightly attenuated) when we use all forested grid cells as the regression sample (Table A.4). Thus, the results do not hinge on restricting attention to the Arc of Deforestation, as we define it.

Fourth, we show that the results are qualitatively similar if we use different thresholds for T^{kill} when defining KDD and measuring extreme heat exposure (see equation 6). The coefficient estimates increase for higher values of T^{kill}, consistent with exposure to higher temperatures having a larger negative effect on crop productivity (Figure A.6).

Finally, to rule out the possibility that the results are picking up spurious correlation with trends in warming (i.e., trends in the first difference of temperature), we show that the results are similar if we include grid cell specific linear trends as controls (Table A.5). This is consistent with the stark timing of the effects displayed in Figure 2, which would be inconsistent with an effect driven by low-frequency trends.

Ruling Out Alternative Mechanisms. In the next section (Section 5) we argue that agricultural expansion is an important mechanism linking temperature extremes to deforestation. Before turning to that analysis, we rule out alternative potential channels.

One possibility is that the main results capture, in part, the effect of deforestation in nearby regions on temperature extremes. Recent work has shown that tree cover can affect weather patterns in down-wind locations (Grosset-Touba et al., 2024) and, most related, Araujo et al. (2023) show that deforestation in the Amazon can lead to further forest loss downwind due to changes in air moisture. To rule out that this is affecting our results, we follow the method of Araujo et al. (2023) to construct a measure of each grid cell's exposure to upwind forest loss (see Appendix C.1). We then control for this measure in estimates of equations (7) and (8). The estimates are very similar to our baseline results, indicating that this mechanism does not drive our findings (see Table A.6).

the future decade.

A second possibility is that our baseline results are capturing direct negative effects of extreme heat on tree health and not human-led deforestation. In the model, this would be captured by extreme heat reducing the cost of deforestation in equation (3). There are several reasons, however, why this mechanism by itself would be inconsistent with the data. First, while this mechanism might explain a contemporaneous relationship between extreme heat and forest loss, it is harder to rationalize how this would lead to additional forest loss for several years (Figure 2). Second, returning to the data on NDVI, we find no evidence that extreme heat reduces NDVI (i.e., worsens tree health) in the deep forest (Figure A.7), suggesting that extreme heat, as we measure it, does not lead to tree "browning" or vegetation loss in regions that are less affected by human activity. Finally, we estimate our main specification in the deep forest and find no evidence that extreme heat affects forest loss there (Figure A.8, third bar), again indicating that extreme heat only affects tree loss in areas with more substantial human activity. More generally, natural forest fires and other forms of non-anthropogenic tree loss in tropical rain forests—the regions that drive our baseline results (see Table 1)—are rare due to high levels of moisture in the environment (e.g., Cochrane, 2003; Andela et al., 2022).[11]

4.3 Extreme Heat and Fire Setting

We next study the effect of extreme heat on fire setting. We do this for three reasons. First, fire setting is an entirely independent measure of land clearing, constructed from different underlying data and image detection methods. This makes it useful validation of our baseline results. Second, forest burning is a particularly damaging form of deforestation because it increases local air pollution and contributes more to carbon emissions. In particular, we note that carbon emissions from tropical forest burning can at their peak be of the same order of magnitude as emissions from global fossil fuel use (e.g., Page et al., 2002). Finally, fire setting is often used to clear land specifically for agriculture due to its short-term soil fertility benefits and the fact that it fully clears the forest floor.

Figure 4a reports estimates of equation (8) in which the outcome variable is the share of burned area in the grid cell. We find that the negative agricultural productivity shock leads to a large, positive contemporaneous effect on burning in the Arc of Deforestation (darkest blue). The lagged estimates suggest that burning does not return fully to its baseline level over the subsequent several years, consistent with the effect on deforestation persisting for several years after the original shock. Comparing these estimates to our main event study

[11] Voiland (2023), a recent NASA Earth Observatory report, writes "In the absence of human activity, fires would not burn in the heart of the Amazon rain forest." Andela et al. (2022) note that "nearly all" fires in the Amazon basin are started by humans.

Figure 4: Extreme Heat and Fire Setting

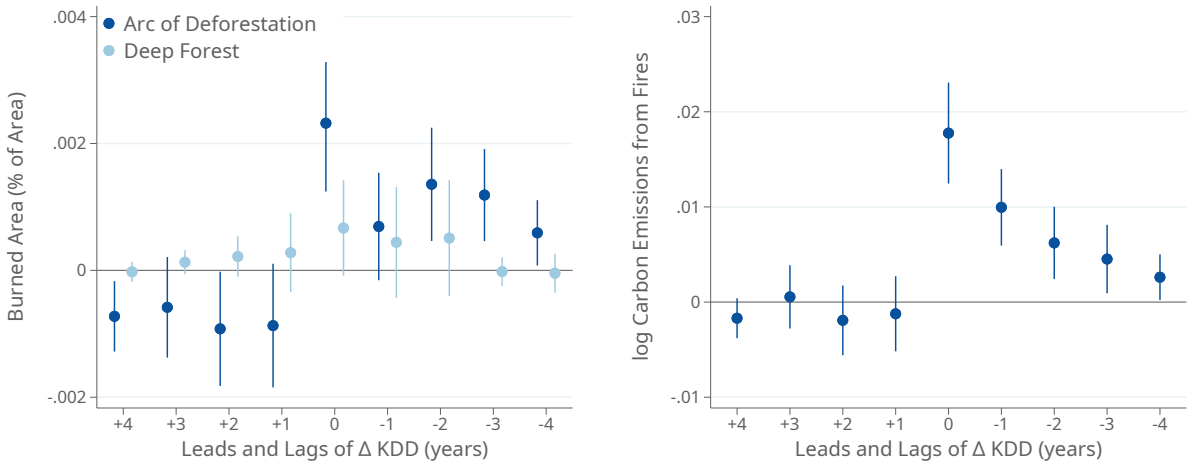

(a) Burned Area (%)

(b) Emissions from Fires

Notes: This figure reports estimates of equation (8) in which the outcome variable is the share of burned area (Figure 4a) and log of estimated carbon emissions from burning (Figure 4b). In Figure 4a, we report separate estimates for grid cells in the Arc of Deforestation and outside the forest. All specifications include grid cell and country-by-year fixed effects. Error bars are 95% confidence intervals based on standard errors clustered by first administrative division (states within countries).

(Figure 2), burning seems to account for roughly one third of the total deforestation effect, and it is concentrated even more in the year of the shock. We again find no evidence of pre-existing trends and little evidence of an effect in deeper in the forest where there is less agricultural activity (light blue). While the contemporaneous and lagged coefficient estimates in the deep forest are positive, they are statistically insignificant and much smaller in magnitude than the effects in the Arc of Deforestation. This suggests that the effect in the Arc of Deforestation is not due to natural causes (e.g., the effect of heat on forest fires) but instead due to human activity.

Figure 4b reports estimates of equation (8) in which the outcome variable is log of total carbon emissions from fires. There is a positive and large contemporaneous effect, which declines in magnitude in subsequent years. This pattern is consistent with denser forested areas and a large share of the organic material being burned in the first year, while burning in subsequent years is for clearing whatever forest remains or increasing soil fertility. The coefficient estimates imply that a one-KDD shock in a given year increases cumulative carbon emissions from fires by over 4%.

4.4 International Spillovers and "Forest Leakage"

So far, we have focused on the relationship between local extreme heat exposure and local deforestation. However, as highlighted by the model, extreme heat can also affect deforestation through global price spillovers (see also Farrokhi et al., 2025). In particular, extreme heat in cell j could affect deforestation in cell i to the extent that lower output in j affects output prices for i.

To investigate this possibility, we measure the extent to which heat shocks elsewhere in the world affect the crops that a given location grows. In particular, we measure

$$\Delta \text{KDD}_{it}^{\text{Spillover}} = \sum_{\text{crop } k} \text{Area}_{ik} \cdot \underbrace{\left(\sum_{j \notin c(i)} \frac{\text{Area}_{jk}}{\sum_{\ell \notin c(i)} \text{Area}_{\ell k}} \Delta \text{KDD}_{jt} \right)}_{\substack{\text{Average shock to crop elsewhere in world} \\ \text{(excluding own country)}}} \tag{9}$$

where Area_{ik} is the area devoted to crop k in cell i, measured using the EarthStat database (Ramankutty et al., 2008) in 2000 (i.e., just prior to our study period). This measure takes on higher values in years when foreign extreme heat shocks hit cells that also cultivate locally grown crops and takes on lower values when foreign extreme heat shocks happen to hit cells that do not cultivate locally grown crops. In the absence of disaggregated, sub-national data on agricultural prices, this measure proxies for the price effects that determined spillovers in the model (Section 2); Hsiao et al. (2025) validate that, at a more aggregated level, a similarly constructed measure of killing degree day exposure on areas planting specific crops predicts world price spikes.

We then estimate an augmented version of our baseline specification that also accounts for foreign spillovers:

$$\text{Deforestation}_{it} = \sum_{j=0}^{4} \beta_j \cdot \Delta \text{KDD}_{i,t-j} + \sum_{j=0}^{4} \tau_j \cdot \Delta \text{KDD}_{i,t-j}^{\text{Spillover}} + \gamma_i + \chi_{c(i),t} + \varepsilon_{it} \tag{10}$$

where now the β_j capture the effect of local extreme heat on deforestation and the τ_j capture the effect of global spillovers. The fact that we exploit differential exposure to foreign shocks across producers of different crops makes it possible to include country-by-time fixed effects $\chi_{c(i),t}$ in the regression, which fully absorb all aggregate fluctuations in heat and deforestation.

Estimates of equation (10) are reported in Figure 5. The first column reports the sum of the β_j (i.e., the effect of local extreme heat exposure after controlling for global spillover effects). The estimate is positive, significant, and similar in magnitude to our

Figure 5: (Lack of) Spillover Effects

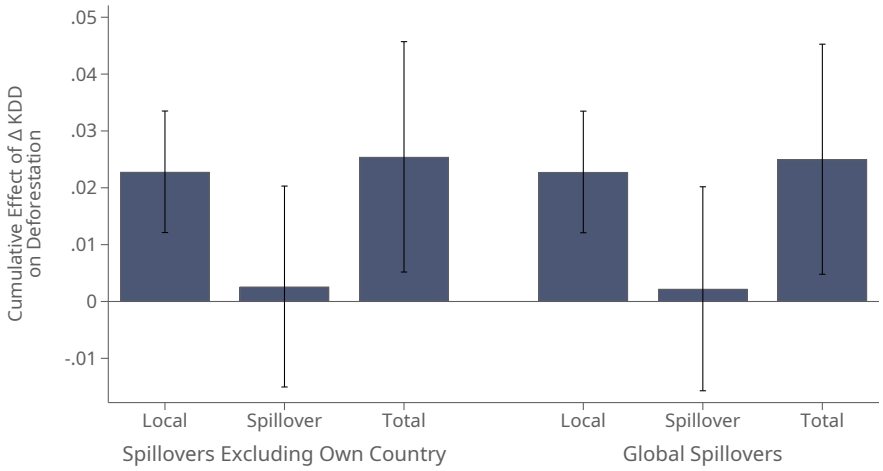

Notes: This figure reports estimates of equation (10). The first and fourth bars report the sum of the β_j; the second and fifth bars report the sum of the τ_j; and the third and sixth bars report the sum of both the β_j and τ_j. In the first set of three bars, the extreme heat spillover is exactly as described in equation (9), while in the second set of three bars we slightly modify it to include extreme heat shocks in other grid cells in the same country. Error bars are 95% confidence intervals based on standard errors clustered by first administrative division (states within countries).

main specification (Table 1), suggesting that our baseline result is not affected by taking spillover effects into account. The second column reports the sum of the τ_j (i.e., the effect of global spillovers). The effect is positive, but small in magnitude and statistically indistinguishable from zero. The third column reports the sum of local and spillover effects and is (intuitively) similar to but slightly larger than the first bar.

Our baseline measure of extreme heat spillovers excludes data from the country in which the grid cell is located. The goal of this approach is to avoid any contamination between the local and global shocks; however, to the extent that the cultivation of specific crops is concentrated in certain countries, this baseline measure may miss an important component of spatial spillovers. To address this issue, the second set of three bars in Figure 5 repeats the same set of estimates except the spillover measure includes shocks to other grid cells in the same country. The results are very similar. Together, these results suggest that "forest leakage" is quantitatively limited and does not seem to meaningfully mediate our results to the degree we can measure it here.

5 Mechanisms: The Borlaug Hypothesis in Action

So far, we have shown that local extreme heat exposure leads to greater deforestation in the Arc of Deforestation, i.e., the global frontier between agricultural lands and forests. This is consistent with a model in which extreme heat reduces local agricultural productivity but nonetheless leads to an expansion of farmland into previously forested areas due to effects on (shadow) prices and/or costs of clearing the forest. In this section, we show direct evidence of each step of that argument. First, we show that the deforestation effects are concentrated in places with the largest heat-induced declines in crop yields by exploiting variation across crops in heat sensitivity. Second, we show that the effects are concentrated in places where food demand is likely to be inelastic. Third, we show direct global evidence of cropland expansion.

5.1 Heterogeneity by Heat Sensitivity and Productivity Effects

We first document that the relationship between extreme heat and deforestation is particularly pronounced in areas that cultivate crops that are most sensitive to heat. We interpret this as evidence that this relationship is driven by declines in agricultural productivity, which should be most pronounced for low-tolerance crops. To implement this test, we exploit variation in temperature sensitivity across crops and variation in baseline cropland allocations across locations, following methods introduced by Moscona and Sastry (2023).

First, we measure crop-specific temperature sensitivity using data from the United Nations Food and Agriculture Organization's EcoCrop database. The EcoCrop data provide information about growing conditions for 2,500 agriculturally important plants, including tolerance ranges for temperature. The key piece of information for our analysis is the reported upper temperature threshold for optimal growing.[12] As examples, wheat (23°C), barley (20°C), and potatoes (25°C) are among the least temperature tolerant crops in our sample, while maize (33°C), sorghum (35°C), sugarcane (37°C), and cotton (36°C) are among the most. Second, we measure the share of each grid cell's land devoted to each crop using the Earthstat database (Ramankutty et al., 2008). These data were created by combining the most detailed census data available for each region with crop-specific potential yield data to construct a 5-by-5 minute grid of the area devoted to each crop circa 2000. We aggregate these data to the one-degree grid level to measure pre-period crop shares.

[12]This database has been used extensively in agronomics and climate science to estimate crop-specific effects of climate change (e.g., Ramirez-Villegas et al., 2013; Hummel et al., 2018). The data are originally compiled from expert surveys and, where possible, from textbooks.

Using these two sources of data, we construct a grid cell-level measure of temperature tolerance as:

$$\text{Temperature Tolerance}_i = \sum_k \text{Share}_{ki} \cdot T_k^{\max} \tag{11}$$

where Share_{ki} is the share of land in i that is devoted to crop k according to Earthstat and $T_k^{\max}$ is the optimal temperature range upper bound of crop k according to Ecocrop. We then estimate an augmented version of equation (8) by interacting the extreme heat shocks with indicators for the bottom quartile and top three quartiles of temperature tolerance:[13]

$$\begin{aligned}\text{Deforestation}_{it} = &\sum_{j=-L}^{K} \left[\beta_j \, \Delta \left(\text{KDD}_{i,t-j} \times \text{Low}_i\right) + \omega_j \, \left(\Delta\text{KDD}_{i,t-j} \times \text{High}_i\right)\right] \\ &+ \gamma_i + \chi_{c(i),t} + \epsilon_{it}\end{aligned} \tag{12}$$

where Low_i and High_i are indicators for low (bottom quartile) and high temperature tolerance locations, respectively. If the main results are driven by declines in agricultural productivity causing land expansion, we would expect the results to be driven by the areas that cultivate crops that are most sensitive to extreme heat. Note also that these results include country-by-year fixed effects, so any estimated effects do not simply reflect differences across different parts of the world.

Our estimates are reported in Figure 6a, which plots the effect of temperature shocks in high and low temperature tolerance locations. The effects are an order of magnitude larger for areas that cultivate low-tolerance crops (dark bars). While we also estimate a positive effect on deforestation for the remainder of the sample (light bars), the effect is much smaller in magnitude. We find no evidence of pre-existing trends in either case.

Thus, extreme heat shocks seem to cause deforestation in precisely the areas where they have the largest negative effect on crop productivity, providing evidence for agricultural productivity as a key mechanism driving deforestation, as in the framework in Section 2. This finding dovetails with our earlier finding that the effect of killing degree days is larger as we choose higher temperature thresholds (Figure A.6), since prior work has documented that crop damage scales with temperature (Schlenker and Roberts, 2009).

[13]The cut-off between these groups is 29.5°C, so areas that exclusively grow any of the low-tolerance or high-tolerance crops mentioned earlier (wheat, barley, or potatoes versus maize, sorghum, sugarcane, or cotton) would be respectively categorized as low and high.

Figure 6: Mechanisms and Heterogeneity

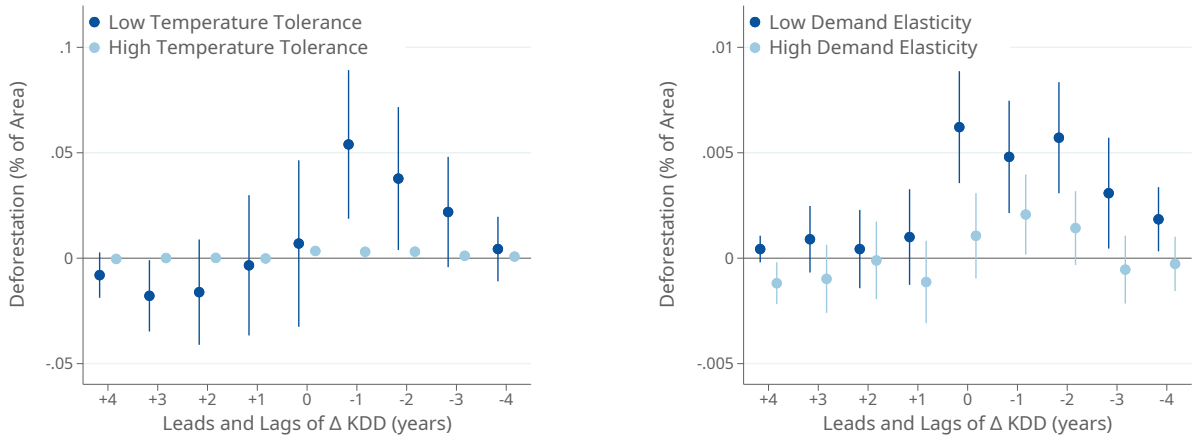

(a) Heterogeneity by Temperature Sensitivity

(b) Heterogeneity by Demand Elasticity

Notes: Each panel reports estimates of equation (12), in which leads and lags of ΔKDD are interacted with indicators for a "high" or "low" attribute. In panel (a), "Low$_i$" corresponds to the bottom quartile of local average temperature sensibility (as described by equation 11) and high to the top three quartiles. In panel (b), "Low$_i$" corresponds to the bottom quartile of the local average food demand elasticity (as described by equation 13). Both models also include grid cell and country-year fixed effects, and the sample is restricted to grid cells within the Arc of Deforestation (see Section 3.3). Error bars are 95% confidence intervals based on standard errors clustered by first administrative division (states within countries).

5.2 Heterogeneity by Demand Elasticity

Our model in Section 2 emphasized that crop price changes are an important mechanism linking adverse productivity shocks to deforestation. Existing work has already documented that crop-level exposure to extreme heat substantially increases crop prices at the country-by-crop level (Hsiao et al., 2025; Crews et al., 2025), consistent with the sign of our main result. We investigate this mechanism in greater detail by exploiting heterogeneity in price elasticities across space. When demand is inelastic, a negative local productivity shock should lead to larger local price increases, leading to greater incentives to clear land for agricultural production. When demand is elastic, on the other hand, prices are less responsive and less likely to compensate for the revenue loss due to lower physical output. This reduces incentives to clear land following an adverse temperature shock.

The ideal data set for investigating this mechanism would be the specific product-level demand elasticity for each grid cell in our sample. However, since those data do not exist, we construct a proxy for local demand elasticities using data from the USDA Commodity and Food Elasticities database. This database compiles demand elasticity estimates from published studies, covering 117 countries and many crops (or groups of crops). We combine these data with pre-period planting patterns from Earthstat, to construct a proxy

for the food demand elasticity of each grid cell:

$$\text{Elasticity}_i = \sum_k \text{Share}_{ki} \cdot \text{Elasticity}_{k,c(i)} \tag{13}$$

where Share_{ki} is the pre-period share of land in i that is devoted to crop k according to Earthstat and $\text{Elasticity}_{k,c(i)}$ is the average demand elasticity for crop k in country c across reported estimates in the USDA database. This proxy based on country-by-crop estimates is imperfect. For instance, it could *over-state* the elasticity of demand in a particularly isolated region of a country that is otherwise open to trade, or *under-state* the elasticity in a country that is closed as a whole but has very integrated within-country markets. Nonetheless, we argue that it is the best measure available at the desired (global) scale.

Our empirical model is the same as equation (12), but with Low_i representing places in the bottom quartile of the distribution of Elasticity_i. If local price effects induced by negative productivity shocks are driving our results, we would expect more pronounced effects in regions with less elastic demand.

We find that extreme heat has a significantly larger marginal effect on deforestation in low-elasticity regions (Figure 6b). While there is also a positive effect in high-elasticity regions, it is smaller in magnitude and only persists for two years following the original shock. This pattern is consistent with the theoretical predictions from Section 2.

As a secondary approach to identify the effect of differences in demand elasticity, we estimate our baseline specification on grid cells of varying sizes. Demand is plausibly more inelastic in larger geographic units compared to smaller ones, which can more easily trade among themselves following a shock.[14] Table A.3 presents our baseline results (Table 1, Panel B) alongside equivalent results estimated at the level of five-by-five degree grid cells and years. The results estimated on the sample of larger grid cells (Panel B) are consistently $\sim$ 30% larger in magnitude than our baseline results (Panel A). While more suggestive, this pattern is also consistent with the predictions of the model.

[14]This approach is related to that of Moscona (2019), which estimates the effect of exogenous changes to agricultural productivity on structural change across both sub-national districts in India and countries. Comparing these sets of estimates sheds light on the key theoretical mechanism linking agricultural productivity shocks to changes in the allocation of land and labor.

5.3 Global Cropland Expansion

We next show directly that extreme heat shocks induce cropland expansion. Using the global land cover data from the ESA, we calculate, for each grid cell i and year t,

$$\text{CroplandExpansion}_{it} = 100 \cdot \frac{\text{CroplandArea}_{it} - \text{CroplandArea}_{i,t-1}}{\text{Area}_i} \tag{14}$$

where CroplandArea_{it} is the measured land cover of cropland in year t and Area_i is the land area of the grid cell. Thus, our measure is in units scaled to the size of the grid cell (in percent values from 0 to 100), and therefore is directly comparable to our measure of deforestation defined in equation (5).

Identifying cropland using satellite imagery is more challenging than identifying forested area for several reasons. Forests are often dense with continuous canopy cover which, combined with the fact that tall and woody vegetation has a characteristic reflectance profile, make them relatively straightforward to detect. Cropland, on the other hand, changes spectral signature dramatically over the course of the year and growing season, and is not as distinct from surrounding pasture or vacant land. Moreover, the spectral signature can vary across crops, land management practices, and field size, making identifying changes in cropland challenging.

We first estimate the dynamic relationship between heat shocks and cropland expansion: that is, equation (8) with CroplandExpansion (equation 14) as the outcome. We find that extreme heat leads to cropland expansion in the Arc of Deforestation (Figure 7a). This effect emerges in the year after the extreme heat shock and persists for several years (dark blue estimates). The finding that cropland expansion is a relatively slower process than deforestation or fire starting (Figures 2 and 4)—i.e., that cropland expansion starts the year after the shock, while deforestation and fire starting begin in the year of the shock—is consistent with the hypothesis that it takes time to convert recently cleared land into farms and that forest has to be cleared before the land can be used for crop agriculture. We find no evidence of pre-existing trends and/or anticipation effects, and no evidence of cropland expansion away from forested areas where opportunities to clear new land are likely more limited (light blue estimates). Consistent with our deforestation results, the effect of extreme heat on cropland expansion is driven by tropical regions (Figure 7b); in fact, we find no evidence that extreme heat causes cropland expansion (as we measure it) outside of tropical countries.

To better capture these delayed dynamic effects, we revisit our long-difference analysis at the grid-cell-by-decade level. Our results, reported in Figure 8, suggest large long-run

Figure 7: Extreme Heat Causes Cropland Expansion: Dynamic Estimates

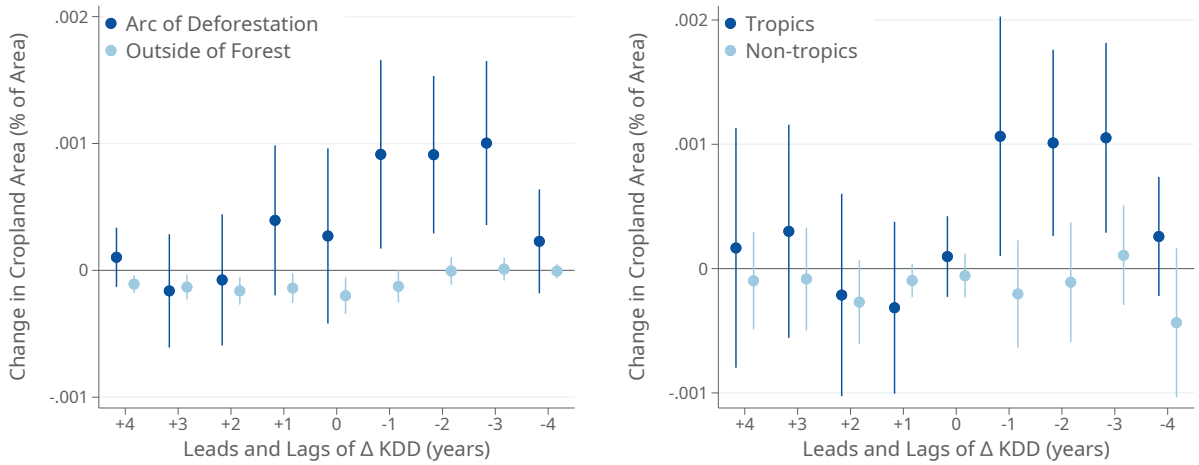

(a) Baseline Effect

(b) Tropics vs. Non-Tropics

Notes: This figure presents the dynamic effects of extreme heat exposure on cropland expansion, defined as in equation (14) using land cover data from the European Space Agency (ESA). The regression equation is a variation of equation (8) with cropland expansion as the outcome. Figure 7a reports estimate of equation (8) for both grid cells in the Arc of Deforestation (dark blue) and grid cells outside the forest (light blue). Figure 7b reports estimate of equation (8) for both grid cells in the Arc of Deforestation in the tropics (dark blue) and grid cells in the Arc of Deforestation outside the tropics (light blue). In addition to the leads and lags of killing degree days, all estimates include grid cell and country-by-year fixed effects. Error bars are 95% confidence intervals based on standard errors clustered by first administrative division (states within countries).

effects of extreme heat on cropland expansion (bar 2) that are of comparable magnitude, in the same land area units, to our earlier findings regarding deforestation (bar 1, reprinting the estimate from Figure 3 for reference). As in our annual estimates, the effect is larger in the tropics than outside the tropics (third and fourth bars) and zero outside of the forest or Arc of Deforestation, where opportunities to clear new land are limited (fifth bar). Taken together, these results support the interpretation that temperature extremes simultaneously induce deforestation and cropland expansion at the edge of tropical forests.

6 Land Use and Input Adjustment: Evidence from Brazil

The analysis thus far has shown that extreme heat leads to more deforestation in the agricultural frontier. Using global satellite data we have shown evidence favoring the "Borlaug hypothesis" mechanism described in Section 2. In particular, we find larger effects in locations suitable for crops that are more temperature sensitive and where demand is more inelastic, and we directly show that cropland indeed expands in the years

Figure 8: Extreme Heat Causes Cropland Expansion: Long-Run Estimates

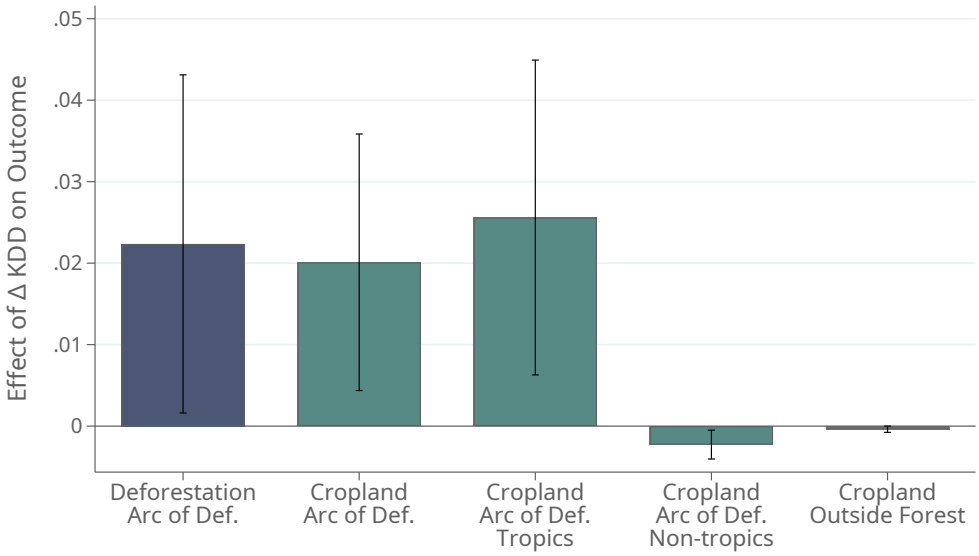

Notes: Each bar reports a separate estimate of equation (7) estimated as a "stacked long difference," with two time periods corresponding respectively to the 2000s and 2010s, and with grid-cell and decade fixed effects. For bar 1, the outcome is deforestation measured from the data of Hansen et al. (2013). For bars 2-5, the outcome is cropland expansion based on the ESA data (Zanaga et al., 2021). Each of these columns varies the sample of the analysis, reported beneath the horizontal axis. Error bars are 95% confidence intervals based on standard errors clustered by first administrative division (states within countries).

after the initial temperature shock.

To probe these effects on agricultural land and input use in more detail, we focus on a deforestation hotspot in which we can study additional agricultural outcomes using census data: Brazil. In particular, we use municipality-level data from the last three rounds of the Brazilian Agricultural Census (1996, 2006, 2017) to study the effect of temperature shocks on several margins of adjustment available to farmers, including but not limited to cropland expansion.

In the census, we measure three variables of interest at the level of municipalities. The first is the total land devoted to both cropland and pasture. The second is the amount of labor devoted to agricultural production, measured in counts of workers. The third is the value of agricultural production in the year of the census. Combining the three census years into a panel, we estimate the following stacked difference model at the level of municipalities i and census rounds t:

$$\Delta \text{Outcome}_{it} = \beta \, \Delta \text{KDD}_{it} + \gamma_i + \chi_t + \epsilon_{it} \tag{15}$$

where the differences are taken between each pair of adjacent censuses and (γ_i, χ_t) are,

Figure 9: Extreme Heat and Agricultural Production in Brazil Using Census Data

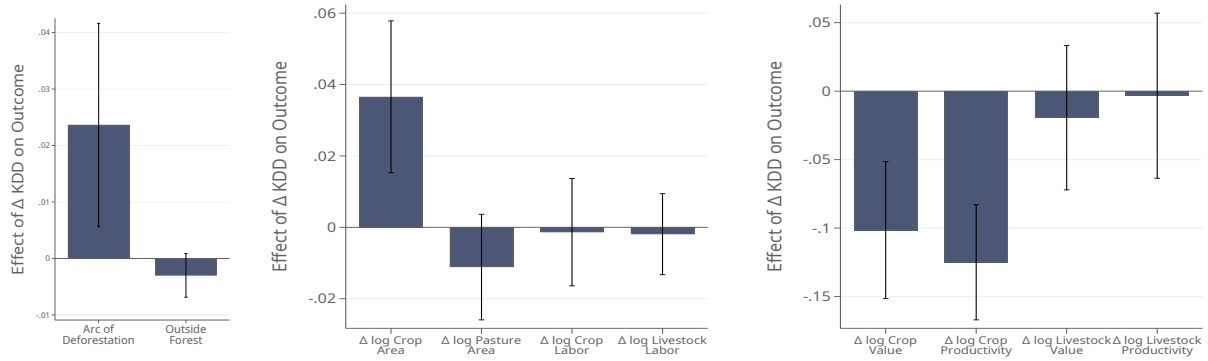

(a) Deforestation **(b)** Land and Labor **(c)** Output Value and Productivity

Notes: Each bar reports a separate estimate of equation (15) with municipality and decade fixed effects, and weighted by total municipality area. In Figure 9a, the years included in the sample are 2001, 2010, and 2019 and the outcome variable is deforestation measured using data from Hansen et al. (2013). In Figures 9b and 9c, the years included in the sample are the Brazilian agricultural census years (i.e., 1996, 2006, and 2017) and each bar corresponds to a different outcome measured from the census, all of which are in log differences, and reported below the x-axis. All specifications restrict attention to municipalities within the Arc of Deforestation, defined as municipalities where a majority of the land area is covered by grid cells in the Arc of Deforestation, using the definition from Section 3.3. Error bars are 95% confidence intervals based on standard errors clustered at the municipality level.

respectively, municipality and time fixed effects. We focus on Brazilian municipalities that are in the Arc of Deforestation by our definition, of which there are about 800 in 2017.

We first reproduce our baseline results on the relationship between deforestation using this empirical framework. Since the Hansen et al. (2013) deforestation data do not exist for 1996, the first Brazilian Agricultural Census round in our sample, we modify (15) slightly to include the years 2001, 2010, and 2019 instead of 1996, 2006, and 2017, but still match the decadal frequency of the panel. The estimates are presented in Figure 9a. Consistent with our baseline results, we find a positive effect of killing degree days on deforestation. This effect is restricted to municipalities in the Arc of Deforestation (bar 1) and we find no evidence of tree cover loss in response to extreme heat away from forested areas (bar 2).

We next investigate how exposure to extreme heat affects agricultural land use using census data. We find that extreme heat drives substantial cropland expansion (Figure 9b, bar 1). One additional KDD per year increases cropland area by 0.036 log points over the decade ($\approx 3.6\%$). By contrast, we find no significant evidence of pasture land expansion (Figure 9b, bar 2). If anything, the coefficient estimate is negative, suggesting that some of the cropland expansion may come at the expense of pasture land in addition to forests. This suggests that heat-induced productivity losses are *not* a major driver of the

expansion of ranching (particularly of cattle) in Brazil, which is a known major contributor to Amazonian deforestation (Assunção et al., 2015; FAO, 2020) but plausibly less sensitive than crop production to rising temperatures.

Do farms intensify production in other ways? The census allows us to also test the effect of extreme heat on agricultural labor use, which has been the predominant focus of existing work in macroeconomics studying the concentration of low-productivity agriculture in poor countries (Gollin et al., 2007) and the implications of climate change for this phenomenon (Nath, 2025). We find no clear evidence that labor use expands, either for crop production (Figure 9b, bar 3) or livestock (Figure 9b, bar 4). The estimates are small in magnitude and statistically indistinguishable from zero. These results suggest that land may be a special and particularly responsive input in the response of agricultural production to climate change.[15] This asymmetry of response between land and labor could arise if extreme heat is a non-neutral shock to the agricultural production function (i.e., it differentially affects the demand for land and labor) and/or if extreme heat has independent effects on the costs of clearing land (e.g., the cost channel in Section 2).

Next, we estimate a negative effect on the value of crop production *despite* this expansion of activity (Figure 9c, bar 1). That is, even though farmers expanded the area under cultivation in response to rising extreme heat exposure, total output declined. Land productivity, defined as production value per unit of area, declines to an even greater extent (bar 2), consistent with greater land area devoted to cropland and expansion of production into *ex ante* more marginal land. The output and productivity of livestock production are both unaffected by extreme heat exposure (Figure 9c, bars 3-4), consistent with our finding of little pasture land adjustment in response to extreme heat exposure.

Finally, we investigate how the main result on cropland expansion varies by farm size. One possibility is that the result is driven by large farms, who are responding to equilibrium price changes and also have the ability to marshal the necessary capital resources for deforestation. Another possibility, however, is that smaller farms drive the effect, potentially through an income effect channel. Figure A.9 reports the effect on cropland separately for the farm size categories that are reported by the Census. The effect is driven by the expansion of cropland in medium and large farms. Moreover, the small and insignificant effects on the bottom two farm size categories suggest that the results are not driven by small farmers clearing forest to recover lost revenue or income.

Together, these findings verify that extreme heat negatively affects crop productivity

[15] It would be interesting to explore the effect of extreme heat on other agricultural inputs beyond land and labor (e.g., tractors, fertilizers). Unfortunately, these data were not collected systematically during the sample period, and were not collected at all for the 1996 census wave, which is necessary for our stacked differences empirical design.

and that the expansion of agricultural inputs does not fully compensate for the lost production. This would be consistent with a case of the model in Section 2 in which productivity declines and local demand is at least partially elastic, so the quantity of agricultural goods produced declines. This evidence would be inconsistent with a case of the model in which the only effect of extreme heat is to lower the cost of clearing the forest, in which case we would expect agricultural production to increase.

7 Quantification and Projections

We finally quantify the aggregate effect of extreme heat on deforestation using a simple, back-of-the-envelope approach. We return to our baseline estimating equation and predict temperature-induced deforestation using local extreme heat exposure:

$$\widehat{\text{Deforestation}}_{it} = \sum_{j=0}^{4} \hat{\beta}_j \Delta \text{KDD}_{i,t-j} \tag{16}$$

where $(\hat{\beta}_j)_{j=0}^4$ are estimated regression coefficients. Predicted deforestation by this definition is in units of percent of a grid cell's land area, and we aggregate this to calculate total deforested area in hectares.

We conduct our analysis in the Global Arc of Deforestation, which our previous analysis suggests is the main frontier of temperature-induced agricultural expansion and consequent deforestation. Motivated by our findings of heterogeneous effects in various deforestation hotspots, we do separate analyses at three geographic levels: the world, the tropics (i.e., areas between the Tropic of Cancer, 23.5° N, and the Tropic of Capricorn, 23.5° S), and Brazil. In each case, we separately estimate the coefficients $(\hat{\beta}_j)_{j=0}^4$ in the respective region to better capture the region-specific effects of extreme heat on deforestation. Conceptually, we think of this heterogeneity as being determined by different agricultural practices (e.g., how temperature tolerant are crops and/or how prevalent is crop vs. animal agriculture), different market structures, and different costs of clearing the world's varied types of forest. These can be thought of as spanning heterogeneity in the productivity effects, price effects, and cost effects identified in the model of Section 2.

The validity of the back-of-the-envelope approach rests on three primary assumptions: the linear functional form of equation (16); the stability of other determinants of deforestation, modeled in the place fixed effects, country-by-time fixed effects, and residual of our empirical model; and the stability of the key estimated regression coefficients that, as mentioned above, embody the various economic mechanisms by which extreme heat

Table 2: The Effects of Extreme Heat on Deforestation in the Arc

		Arc of Deforestation in		
		World	Tropics	Brazil
Panel A: In-Sample 2006-2019	Total Effect (million ha)	1.42	1.28	1.20
	% of In-Sample Deforestation	1.33%	2.04%	8.17%
	% of Initial Forest	0.12%	0.19%	0.99%
Panel B: Out of Sample 2020-2099 (SSP245)	Total Effect (million ha)	28.1	30.3	19.7
	% of In-Sample Deforestation	26.3%	48.1%	134%
	% of Initial Forest	2.42%	4.57%	15.8%
Panel C: Out of Sample 2020-2099 (SSP585)	Total Effect (million ha)	90.7	95.8	57.9
	% of In-Sample Deforestation	84.8%	152.1%	393.6%
	% of Initial Forest	7.8%	14.4%	46.3%

Notes: This table reports our predictions for the effect of extreme heat on deforestation. Panel A corresponds to calculations in-sample, from 2006 to 2019, and Panel B and Panel C correspond to calculations out of sample, based on Coupled Model Intercomparison Project Phase 6 (CMIP6) model at SSP245 and SSP585 scenario, respectively. The three columns correspond to analyses corresponding to the whole world, the tropics, and Brazil. In each case, we restrict analysis to the Arc of Deforestation (see Section 3.3). The total effect is reported in millions of hectares. The "% of In-Sample Deforestation" is reported as a percent of the total forest loss according to Hansen et al. (2013) in the relevant area. This can exceed 100% when comparing predicted climate-induced deforestation to observed deforestation. The "% of Initial Forest" is scaled to the initial forested area in 2000 (Panel A) or 2023 (Panel B and Panel C).

affects deforestation. We note that all three assumptions are more likely to be valid for in-sample analysis than for out-of-sample extrapolation to model probable future climate change. We return to this point below in our discussion.

In-Sample Analysis. We first use the model to predict how adverse temperature shocks affected global deforestation during the sample period (Table 2, Panel A). Extreme heat exposure caused 1.42 million hectares of deforestation, an area roughly the size of Connecticut or Northern Ireland, or over one thousand square kilometers per year. The vast majority took place in the tropics (1.28 million hectares) and in Brazil in particular (1.20 million hectares). Within the Arc of Deforestation, this effect of extreme heat accounts for 2% of all tropical deforestation and over 8% of all Brazilian deforestation. In the Brazilian Arc of Deforestation, extreme heat exposure from 2005 to 2019 led to the destruction of 1% of all forest cover.

End-of-century Analysis. We next combine our estimates with temperature realization projections through 2100 in order to better understand how future trends in extreme heat exposure may accelerate global deforestation. To approximate future extreme heat exposure, we use future temperature projections from an ensemble of global climate models

from the Coupled Model Intercomparison Project Phase 6 (CMIP6; see Appendix C.2). Following existing literature (e.g., Hultgren et al., 2025), we focus on shared socioeconomic pathway (SSP) 2-4.5 as an approximation of a "middle of the road" scenario and SSP 5-8.5 as an approximation of a high emissions scenario. We then combine these projections from each year with the coefficient estimates from our baseline panel specification in order to quantify the impact of future warming on forest loss through 2100. The results are presented in Table 2, Panels B and C.

By the end of the century, a middle of the road warming scenario implies that extreme heat will lead to the deforestation of over 28 million hectares (Panel B). While this forest loss takes place over a longer period of time than our regression sample, these estimates imply that the annual rate of heat-induced deforestation will increase by roughly three fold. If we instead assume a high emissions scenario, extreme heat will lead to the deforestation of 90 million hectares. The effect is again stronger in the tropics, which will lose 5% or 14% (depending on the emissions scenario) of its Arc of Deforestation through this mechanism. The effects are again even starker in the Brazilian Arc, which will lose 16% or as much as 46% of its forest cover due to these land use adjustments to extreme heat. These numbers are all large when compared to deforestation that has taken place to date; for example, the more conservative estimates from Panel B imply that future heat-induced deforestation will amount to 48% of tropical deforestation that took place from 2006 to 2019 and 134% of Brazilian deforestation that took place from 2006 to 2019. Together, these findings suggest that the rise in extreme heat exposure projected to take place in the coming decades could lead to substantial forest loss and dramatically accelerate the current rate of deforestation.

Discussion. As noted above, the out-of-sample projections require a stronger set of assumptions than the in-sample analysis. A key question is whether the observed relationship between negative temperature shocks to agricultural productivity and deforestation continues to hold in the future. As highlighted by the model in Section 2, this may not be the case if either the marginal effect of extreme heat on agricultural productivity declines in absolute value (e.g., if farmers around the world adopt more resilient technology), or if prices become less responsive to local changes in agricultural productivity (e.g., if global agricultural markets become more integrated).

While changes in both are possible, recent trends do not point in the direction of either. First, Burke and Emerick (2016) find no evidence that the marginal effect of extreme heat on crop productivity has declined over recent decades, and Moscona and Sastry (2023) find that only a small share of the negative effect of extreme heat on agricultural productivity has been mitigated by new technology development. Both papers focus on the US, which may be the country where changes in production resilience are most likely,

due to its role as a leader in agricultural biotechnology. Second, agricultural markets have (if anything) become less (not more) integrated in recent years. This pattern may continue as a growing number of countries promote self sufficiency in food production, especially in tropical regions where the results are concentrated. In fact, recent evidence suggests that global warming itself has led to a greater number of restrictions on trade in agricultural commodities and lower overall trade volumes (Hsiao et al., 2025). This suggests that there may be even larger effects of extreme heat on deforestation in the future than there have been to date. Nevertheless, the end-of-century estimates should be interpreted with greater caution than the estimates from the regression sample.

8 Conclusion

A large literature has arisen to investigate the impact of rising temperatures on agriculture, concluding that heat causes severe damage to agricultural productivity when and where it occurs (e.g., Lobell and Field, 2007; Schlenker and Roberts, 2009; Lobell et al., 2011; Hultgren et al., 2025). But then what will happen? One view emphasizes reallocation away from agricultural production in heat-exposed regions, such that endogenous land use changes mitigate the economic consequences of climate change and reduce deforestation in the tropical regions that are most affected by global warming. An alternative possibility, however, is that farmers double down in regions affected by climate change. That is, they expand land under cultivation by deforesting more, even at lower productivity. In doing so, they effectively increase–rather than decrease—their exposure to rising temperatures. This idea is consistent with the original "Borlaug hypothesis," which asserts that productivity gains from technological improvements could reduce deforestation as farmers grow more with less land (Borlaug, 2000). Applying this same logic to climate change, productivity losses could increase deforestation as farmers can grow less with the land that they have, and then seek out even more land on which to grow. In turn, increased deforestation releases carbon emissions that accelerate climate change.

This paper empirically investigates the relationship between global warming and deforestation. We show that extreme heat increases deforestation by lowering agricultural productivity and inducing cropland expansion at the forest frontier. Combining global data on daily temperature realizations and deforestation, we find that exposure to killing degree days persistently raises forest loss, especially in tropical regions, and can be explained largely by cropland expansion. These findings are corroborated by an analysis of Brazilian agricultural census data, which shows that extreme heat causes decade-long declines in agricultural productivity and cropland expansion, while generating little ad-

justment along other margins.

Our estimates imply that extreme heat caused nearly 1.5 million hectares of forest loss from 2005 to 2019 and could lead to an additional 28 million by 2100, amounting to over 26% of all deforestation and 48% of tropical deforestation that took place during the sample period. These findings underscore the need to incorporate endogenous land-use responses into models of climate damages and to align agricultural and conservation policies in a warming world. Our results suggest that adverse productivity shocks will heighten local incentives to clear land, challenging the more optimistic view that endogenous land use changes will counteract the economic and environmental damages from climate change.

References

Abman, R. and Carney, C. (2020). Agricultural productivity and deforestation: Evidence from input subsidies and ethnic favoritism in Malawi. *Journal of Environmental Economics and Management*, 103:102342.

Abman, R., Garg, T., Pan, Y., and Singhal, S. (2020). Agricultural productivity and deforestation. *Available at SSRN 3692682*.

Akerman, A. (2025). Deforestation and the demographic transition: Lessons from Brazil. Working paper, Boston University.

Andela, N., Morton, D. C., Schroeder, W., Chen, Y., Brando, P. M., and Randerson, J. T. (2022). Tracking and classifying amazon fire events in near real time. *Science advances*, 8(30):eabd2713.

Araujo, R., Assunção, J., Hirota, M., and Scheinkman, J. A. (2023). Estimating the spatial amplification of damage caused by degradation in the Amazon. *Proceedings of the National Academy of Sciences*, 120(46):e2312451120.

Assunção, J., Gandour, C., and Rocha, R. (2015). Deforestation slowdown in the Brazilian Amazon: Prices or policies? *Environment and Development Economics*, 20(6):697–722.

Assunção, J., Gandour, C., and Rocha, R. (2023). DETER-ing deforestation in the amazon: environmental monitoring and law enforcement. *American Economic Journal: Applied Economics*, 15(2):125–156.

Balboni, C., Berman, A., Burgess, R., and Olken, B. (2023). The economics of tropical deforestation. *Annual Review of Economics*, 15:723–754.

Barrett, C. B. (1999). Stochastic food prices and slash-and-burn agriculture. *Environment and Development Economics*, 4(2):161–176.

Barrozo, M. (2025). Where is the beef? supply chains and carbon emissions in the amazon. Working paper, DePaul University.

Beyer, R. M., Hua, F., Martin, P. A., Manica, A., and Rademacher, T. (2022). Relocating croplands could drastically reduce the environmental impacts of global food production. *Communications Earth & Environment*, 3(1):49.

Borlaug, N. E. (2000). The Green Revolution revisited and the road ahead. Nobel Lecture, Oslo, Norway, December 8, 2000. Accessed 2025-10-07.

Burgess, R., Costa, F., Hsiao, A., Olken, B., and Salazar Restrepo, V. (2025). The political economy of conservation.

Burgess, R., Costa, F., and Olken, B. (2024). National borders and the conservation of nature. Working paper, London School of Economics.

Burgess, R., Hansen, M., Olken, B., Potapov, P., and Sieber, S. (2012). The political economy of deforestation in the tropics. *Quarterly Journal of Economics*, 127(4):1707–1754.

Burke, M. and Emerick, K. (2016). Adaptation to climate change: Evidence from US agriculture. *American Economic Journal: Economic Policy*, 8(3):106–140.

Butler, E. E. and Huybers, P. (2013). Adaptation of US maize to temperature variations. *Nature Climate Change*, 3(1):68–72.

Carleton, T., Crews, L., and Nath, I. (2025). Agriculture, trade, and the spatial efficiency of global water use.

Carreira, I., Costa, F., and Pessoa, J. P. (2024). The deforestation effects of trade and agricultural productivity in brazil. *Journal of development economics*, 167:103217.

Chen, Y., Hall, J., van Wees, D., Andela, N., Hantson, S., Giglio, L., van der Werf, G. R., Morton, D. C., and Randerson, J. T. (2023). Multi-decadal trends and variability in burned area from the fifth version of the global fire emissions database (gfed5). *Earth System Science Data*, 15(11):5227–5259.

Cochrane, M. A. (2003). Fire science for rainforests. *Nature*, 421(6926):913–919.

Costa, F., Hsiao, A., Pellegrina, H., and Souza-Rodrigues, E. (2025). Deforestation. *VoxDevLit*, 18(1).

Costinot, A., Donaldson, D., and Smith, C. (2016). Evolving comparative advantage and the impact of climate change in agriculture. *Journal of Political Economy*, 124(1):205–248.

Crews, L., Nath, I., Schmitz, A., and Stewart, S. (2025). Trade policy and food security with climate and geopolitical risk. Work in progress, UCLA.

Cruz, J.-L. and Rossi-Hansberg, E. (2024). The economic geography of global warming. *Review of Economic Studies*, 91(2):899–939.

Csillik, O., Keller, M., Longo, M., Ferraz, A., Rangel Pinagé, E., Görgens, E. B., Ometto, J. P., Silgueiro, V., Brown, D., Duffy, P., et al. (2024). A large net carbon loss attributed to anthropogenic and natural disturbances in the amazon arc of deforestation. *Proceedings of the National Academy of Sciences*, 121(33):e2310157121.

Davis, K. F., Rulli, M. C., Seveso, A., and D'Odorico, P. (2017). Increased food production and reduced water use through optimized crop distribution. *Nature Geoscience*, 10(12):919–924.

FAO (2020). *The State of the World's Forests 2020: Forests, Biodiversity and People*. FAO and United Nations Environment Programme, Rome. Accessed: October 12, 2025.

Farrokhi, F., Kang, E., Pellegrina, H., and Sotelo, S. (2025). Deforestation: A global and dynamic perspective. Technical Report 34150, National Bureau of Economic Research.

Fearnside, P. M. (2005). Deforestation in brazilian amazonia: history, rates, and consequences. *Conservation biology*, 19(3):680–688.

Gollin, D., Parente, S. L., and Rogerson, R. (2007). The food problem and the evolution of international income levels. *Journal of Monetary Economics*, 54(4):1230–1255.

Grosset-Touba, F., Papp, A., and Taylor, C. (2024). Rain follows the forest: Land use policy, climate change, and adaptation. SSRN Working Paper, Posted January 27, 2023; Last revised January 13, 2024.

Hansen, M. C., Potapov, P. V., Moore, R., Hancher, M., Turubanova, S. A., Tyukavina, A., Thau, D., Stehman, S. V., Goetz, S. J., Loveland, T. R., et al. (2013). High-resolution global maps of 21st-century forest cover change. *Science*, 342(6160):850–853.

Hertel, T. (2002). Applied general equilibrium analysis of agricultural and resource policies. In Gardner, B. and Rausser, G., editors, *Handbook of Agricultural Economics*, volume 2A, pages 1373–1419.

Hertel, T. (2013). Global applied general equilibrium analysis using the global trade analysis project framework. In Dixon, P. and Jorgenson, D., editors, *Handbook of Computable General Equilibrium Modeling*, volume 1, pages 815–876.

Hsiao, A. (2025). Coordination and commitment in international climate action: Evidence from palm oil. Working paper, Stanford University.

Hsiao, A., Moscona, J., and Sastry, K. (2025). Food policy in a warming world. Working Paper 32539, National Bureau of Economic Research.

Hultgren, A., Carleton, T., Delgado, M., Gergel, D. R., Greenstone, M., Houser, T., Hsiang, S., Jina, A., Kopp, R. E., Malevich, S. B., et al. (2025). Impacts of climate change on global agriculture accounting for adaptation. *Nature*, 642(8068):644–652.

Hummel, M., Hallahan, B., Brychkova, G., Ramirez-Villegas, J., Guwela, V., Chataika, B., Curley, E., McKeown, P., Morrison, L., Talsma, E., et al. (2018). Reduction in nutritional quality and growing area suitability of common bean under climate change induced drought stress in Africa. *Scientific Reports*, 8(1):16187.

Jones, B. F., Moscona, J., Olken, B. A., and von Dessauer, C. (2025). With or Without U? Binning Bias and the Causal Effects of Temperature Shocks. Working Paper.

Lobell, D. and Field, C. (2007). Global scale climate-crop yield relationships and the impacts of recent warming. *Environmental Research Letters*, 2(1):014002.

Lobell, D., Schlenker, W., and Costa-Roberts, J. (2011). Climate trends and global crop production since 1980. *Science*, 333(6042):616–620.

Matsuyama, K. (1992). Agricultural productivity, comparative advantage, and economic growth. *Journal of Economic Theory*, 58(2):317–334.

Mishra, P. (2025). The global allocative efficiency of deforestation. Working paper, Wharton School.

Moscona, J. (2019). Agricultural development and structural change within and across countries. Working paper, MIT.

Moscona, J. and Sastry, K. (2023). Does directed innovation mitigate climate damage? evidence from US agriculture. *Quarterly Journal of Economics*, 138(2):637–701.

Moscona, J. and Sastry, K. A. (2025). Inappropriate technology: Evidence from global agriculture. Working Paper 33500, National Bureau of Economic Research.

Muñoz Sabater, J., Dutra, E., Agustí-Panareda, A., Albergel, C., Arduini, G., Balsamo, G., Boussetta, S., Choulga, M., Harrigan, S., Hersbach, H., Martens, B., Miralles, D. G., Piles, M., Rodríguez-Fernández, N. J., Zsoter, E., Buontempo, C., and Thépaut, J.-N. (2021). Era5-land: A state-of-the-art global reanalysis dataset for land applications. *Earth System Science Data*, 13(9):4349–4383.

Nath, I. (2025). Climate change, the food problem, and the challenge of adaptation through sectoral reallocation. *Journal of Political Economy*, 133(6):1705–1756.

Page, S. E., Siegert, F., Rieley, J. O., Boehm, H.-D. V., Jaya, A., and Limin, S. (2002). The amount of carbon released from peat and forest fires in indonesia during 1997. *Nature*, 420(6911):61–65.

Pelletier, J., Ngoma, H., Mason, N. M., and Barrett, C. B. (2020). Does smallholder maize intensification reduce deforestation? evidence from zambia. *Global Environmental Change*, 63:102127.

Ramankutty, N., Evan, A. T., Monfreda, C., and Foley, J. A. (2008). Farming the planet: 1. geographic distribution of global agricultural lands in the year 2000. *Global Biogeochemical Cycles*, 22(1):GB1003.

Ramirez-Villegas, J., Jarvis, A., and Läderach, P. (2013). Empirical approaches for assessing impacts of climate change on agriculture: The EcoCrop model and a case study with grain sorghum. *Agricultural and Forest Meteorology*, 170:67–78.

Rising, J. and Devineni, N. (2020). Crop switching reduces agricultural losses from climate change in the united states by half under rcp 8.5. *Nature Communications*, 11(1):4991.

Schlenker, W. and Roberts, M. J. (2009). Nonlinear temperature effects indicate severe damages to us crop yields under climate change. *Proceedings of the National Academy of sciences*, 106(37):15594–15598.

Schultz, T. W. (1953). *The economic organization of agriculture*. McGraw Hill, New York.

Szerman, D., Assunção, J., Lipscomb, M., and Mobarak, A. M. (2024). Electricity, agricultural productivity, and deforestation: Evidence from brazil. Working paper, September 18, 2024.

Voiland, A. (2023). Drought fuels wildfires in the amazon. NASA Earth Observatory. Published October 11, 2023; accessed on [insert access date].

Zanaga, D., Van De Kerchove, R., De Keersmaecker, W., Souverijns, N., Brockmann, C., Quast, R., Wevers, J., Grosu, A., Paccini, A., Vergnaud, S., Cartus, O., Santoro, M., Fritz, S., Georgieva, I., Lesiv, M., Carter, S., Herold, M., Li, L., Tsendbazar, N. E., Ramoino, F., and Arino, O. (2021). ESA WorldCover 10 m 2020 v100. Zenodo. Dataset. European Space Agency WorldCover project.

Appendix

A Supplementary Figures and Tables

Figure A.1: Dynamic Effect of Extreme Heat on NDVI

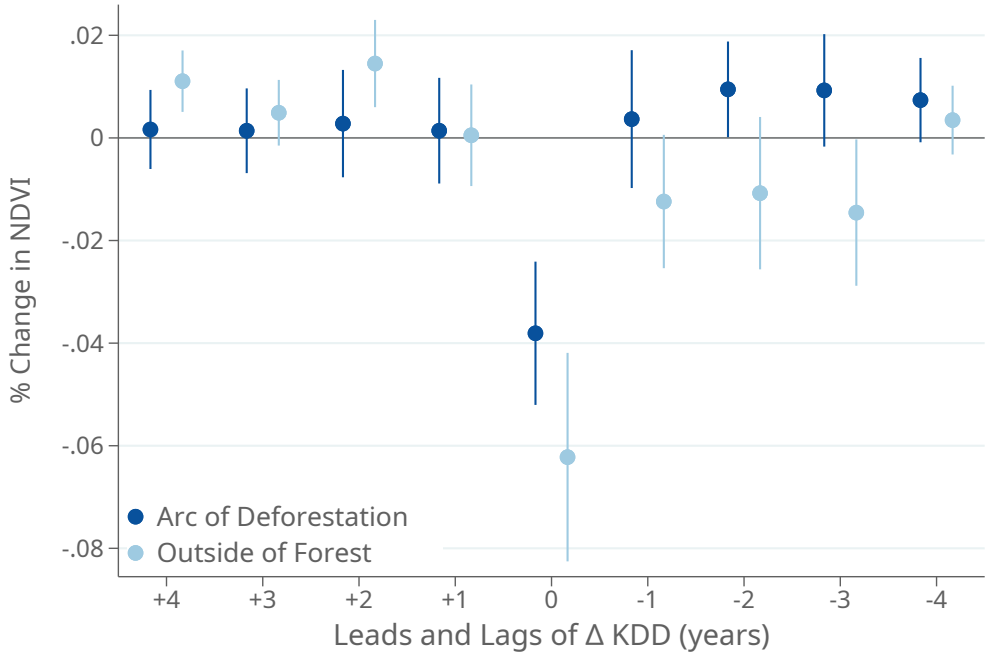

Notes: This plot reports coefficient estimates from equation (8) in which the outcome variable is the percent change in NDVI, $100 \cdot ((\text{NDVI}_{it} - \text{NDVI}_{i,t-1})/\text{NDVI}_{it-1})$, and the sample is restricted to grid cells that contain cropland. The dark blue coefficients are from estimates on the sample of grid cells inside the Arc of Deforestation and the light blue coefficients are from estimates on the sample of grid cells outside of the forest (see Section 3.3). Error bars are 95% confidence intervals based on standard errors clustered by first-level administrative division (states within countries).

Figure A.2: Extreme Heat Causes Deforestation: Levels Specification

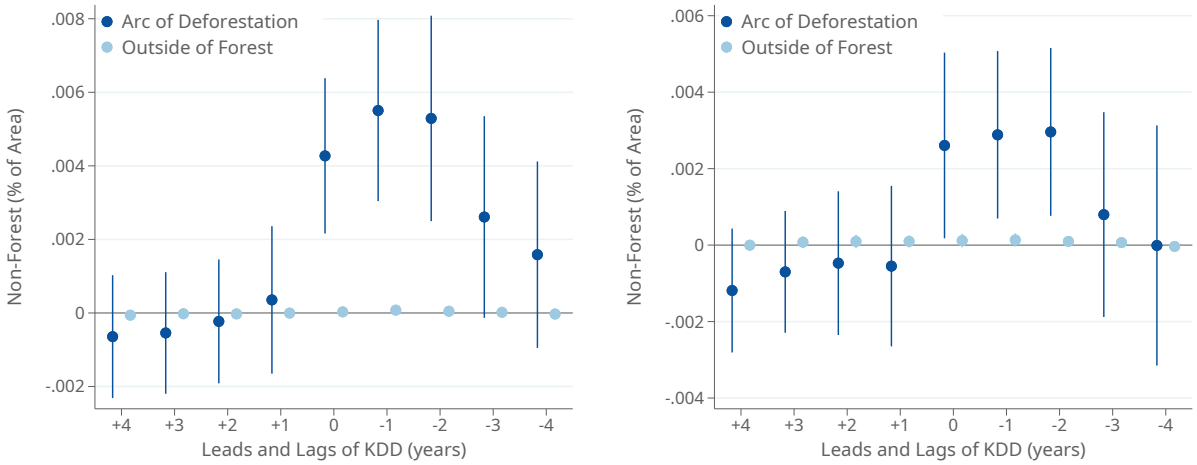

(a) Cell and Year Fixed Effects

(b) Cell and Country-Year Fixed Effects

Notes: This figure plots coefficients from a variant of our dynamic event study (equation 8) estimated in levels. That is, the outcome is the share of the grid cell not covered by trees (in units of percent of grid cell; i.e., the variable of which $\text{Deforestation}_{it}$, defined in equation 5, is the first difference) and the main regressors are leads and lags of KDD_{it}. Each sub-figure reports estimates on two different samples: the Arc of Deforestation, in dark blue, and areas outside the forest, in light blue (see Section 3.3). In addition to the leads and lags of killing degree days, the estimates in Figure A.2a include grid cell and year fixed effects and the estimates in Figure A.2b include grid cell and country-by-year fixed effects. Error bars are 95% confidence intervals based on standard errors clustered by first-level administrative division (states within countries).

Figure A.3: Extreme Heat Causes Deforestation: Outcome as log Deforestation

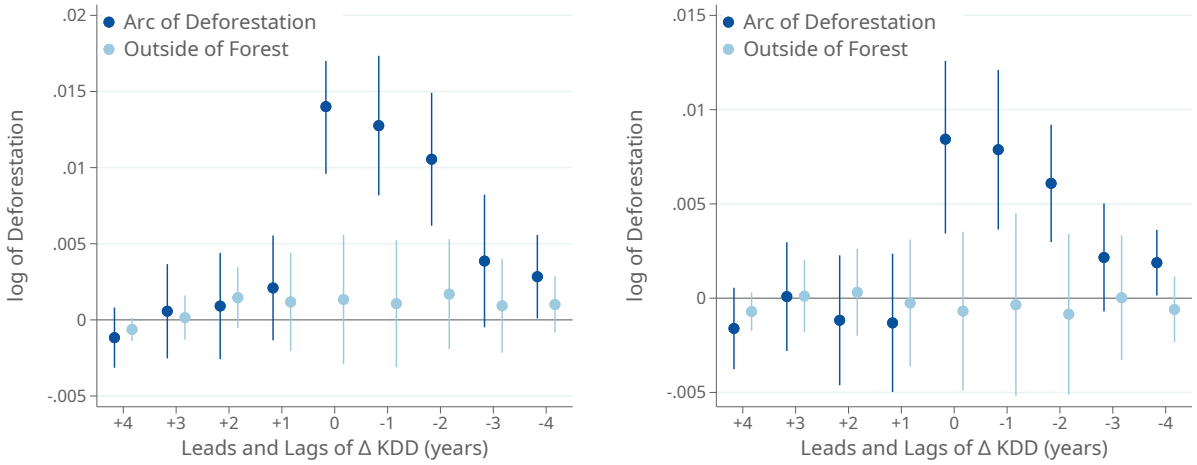

(a) Cell and Year Fixed Effects

(b) Cell and Country-Year Fixed Effects

Notes: This figure presents the dynamic effects of extreme heat exposure on deforestation, in a variant model where the outcome variable is in logarithms. Each sub-figure reports estimate of this variant of equation (8) on two different samples: the Arc of Deforestation, in dark blue, and areas outside the forest, in light blue (see Section 3.3). In addition to the leads and lags of killing degree days, the estimates in Figure A.3a include grid cell and year fixed effects and the estimates in Figure A.3b include grid cell and country-by-year fixed effects. Error bars are 95% confidence intervals based on standard errors clustered by first-level administrative division (states within countries).

Figure A.4: The Persistence of KDD Shocks

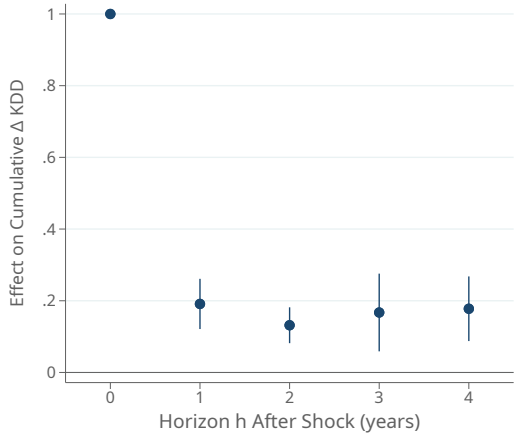

Notes: This figure presents estimates of the regression model,

$$\text{KDD}_{i,t+h} - \text{KDD}_{i,t-1} = \beta_{0,h}\Delta\text{KDD}_{it} + \sum_{j=1}^{4}\beta_{j,h}\Delta\text{KDD}_{i,t-j} + \gamma_i + \chi_{c(i),t} + \epsilon_{it}$$

The regression sample is the Arc of Deforestation, as defined in Section 3.3, and the model includes grid-cell and country-by-time fixed effects. Each point shows the estimate of $\beta_{0,h}$, the marginal effect of ΔKDD_{it}, from a separate projection regression. Error bars are 95% confidence intervals based on standard errors clustered by first-level administrative division (states within countries).

Figure A.5: Testing for Pre-trends in the Decadal-Frequency Relationship between Extreme Heat and Deforestation

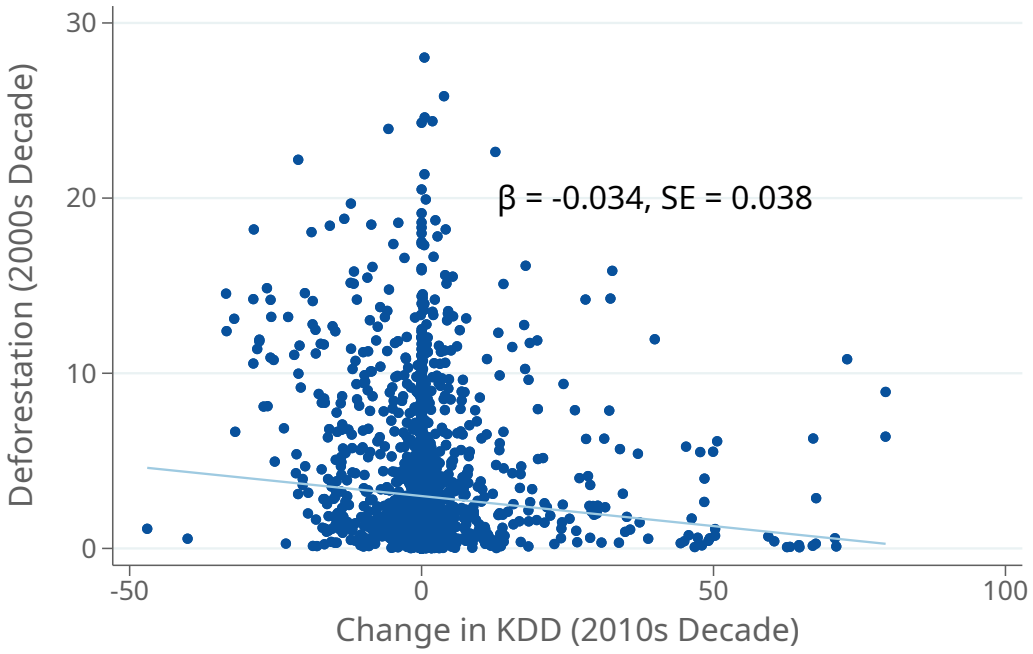

Notes: This figure reports estimates of the scatter plot corresponding to the following regression specification:

$$\text{Deforestation}_{i,2000s} = \beta \cdot \Delta\text{KDD}_{i,2010s} + \varepsilon_{it}$$

where the vertical axis is deforestation during the 2000s decade and the horizontal axis is the change in KDDs during the 2010s decade. Standard errors are clustered by country.

Figure A.6: Effects by Killing Degree Day Threshold

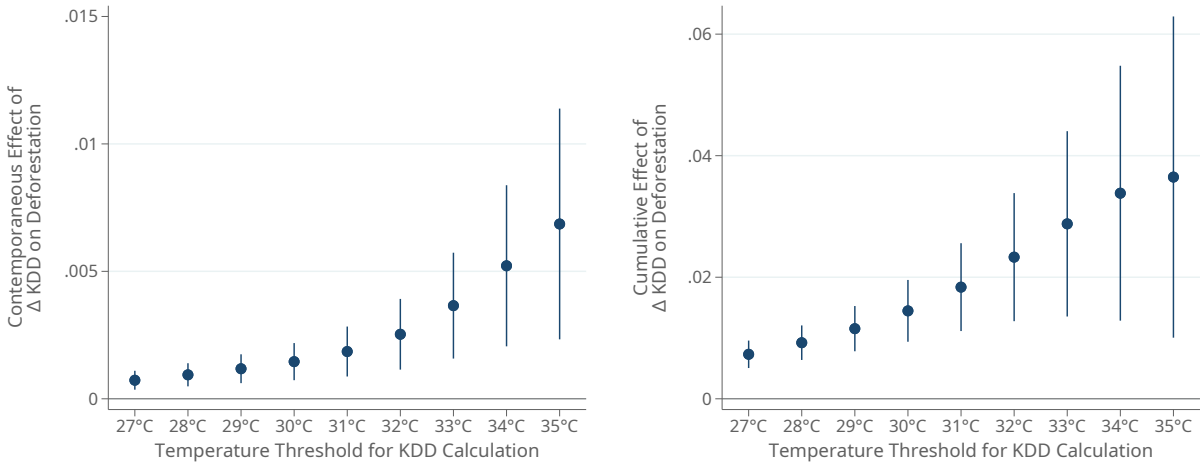

(a) Contemporaneous Effect **(b)** Cumulative Effect

Notes: Panel (a) reports estimates of equation (7) in which killing degree days are constructed with different values for T^{kill} (see equation 6). The value of T^{kill} in each specification is listed on the x-axis. Panel (b) reports cumulative effects of the contemporaneous effect and four lags using estimates of (8). Error bars are 95% confidence intervals based on standard errors clustered by first-level administrative division (states within countries).

Figure A.7: NDVI Effects by Forest Section

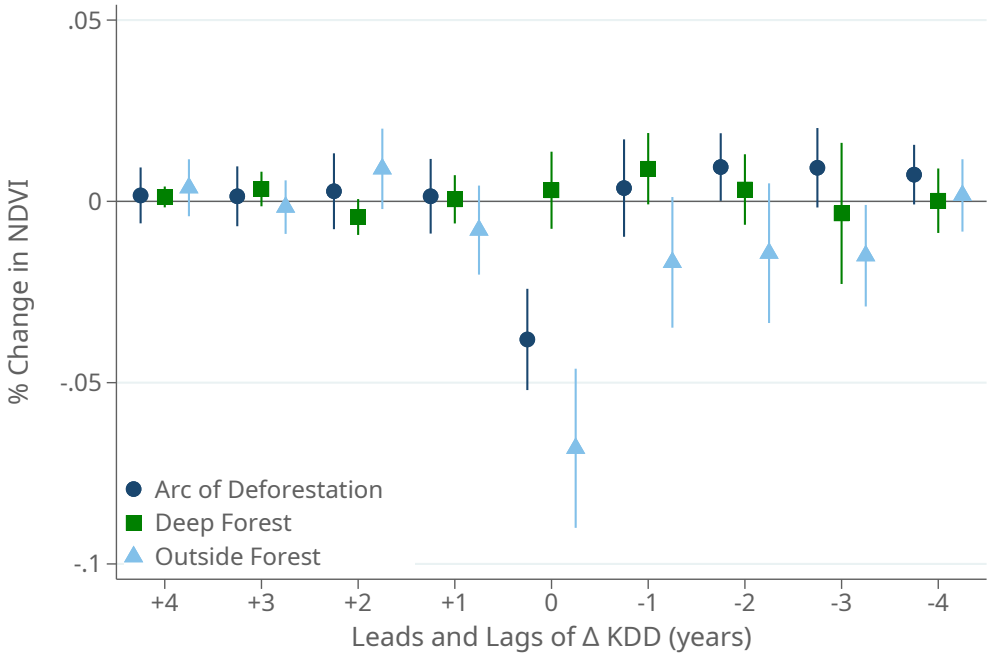

Notes: This plot reports coefficient estimates from equation (8) in which the outcome variable is the percent change in NDVI, $100 \cdot ((\text{NDVI}_{it} - \text{NDVI}_{i,t-1})/\text{NDVI}_{it-1})$. Each set of coefficients corresponds to estimates from a different sample: the Arc of Deforestation (dark blue circles), the deep forest (green squares) and non-forested area (light blue triangles), all of which are defined in Section 3.3. Error bars are 95% confidence intervals based on standard errors clustered by first-level administrative division (states within countries).

Figure A.8: The Effects of Extreme Heat on Deforestation by Forest Section

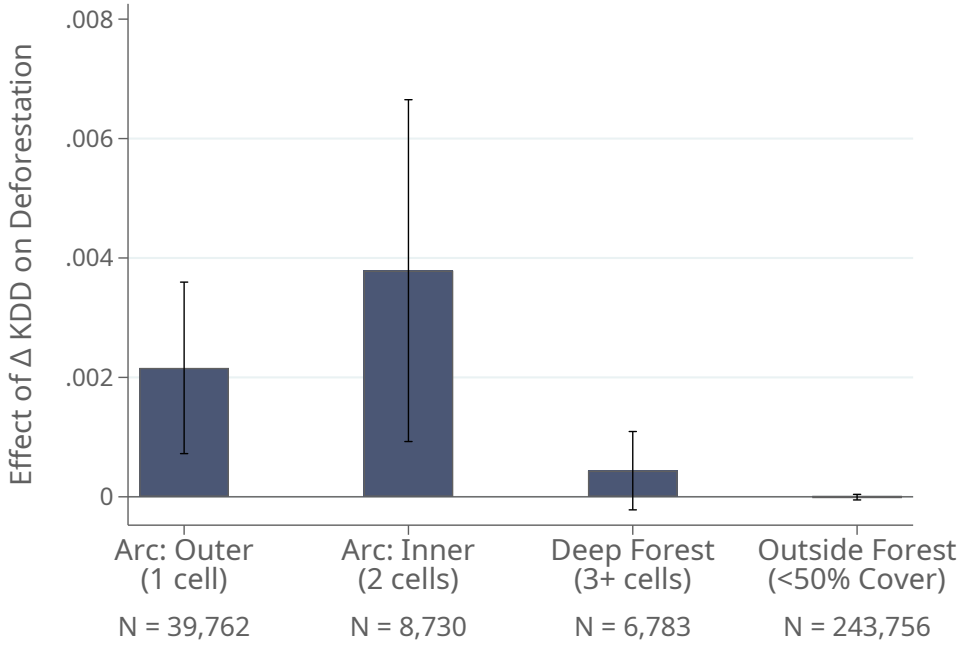

Notes: This figure reports estimates of equation (7) restricting attention to different samples. We define "the forest" as grid cells with more than 50% tree canopy cover. We separate the forest into layers based on the distance (in grid cells) to the edge of the forest (columns 1-3), where the first two columns together constitute our definition of the Arc of Deforestation and the third column is our definition of the Deep Forest. The sample in the fourth bar is all non-forest grid cells ($< 50\%$ tree canopy cover). Error bars are 95% confidence intervals based on standard errors clustered by first-level administrative division (states within countries).

Figure A.9: Effects on Cropland Expansion in Brazil by Farm Size

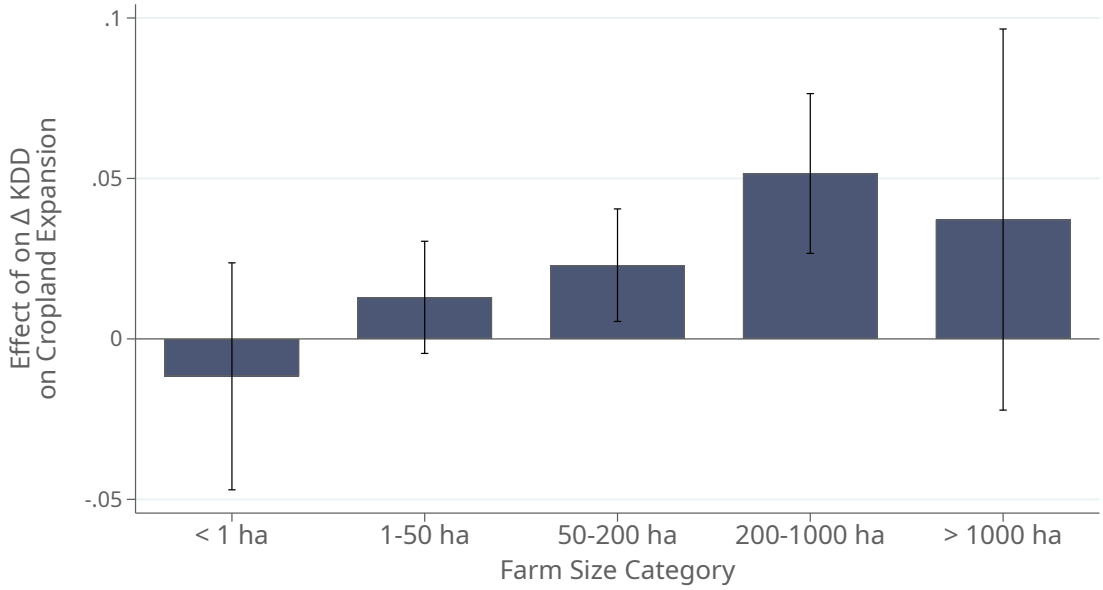

Notes: This figure reports estimates of equation (15) in which the outcome variable is (log of the) cropland area in farms of different sizes, reported on the horizontal axis. All specifications include municipality and decade fixed effects, and the sample is restricted to municipalities inside Brazil's Arc of Deforestation. Error bars are 95% confidence intervals based on standard errors clustered by municipality.

Table A.1: Temperature Extremes Cause Deforestation: ESA Measurement

	(1)	(2)	(3)	(4)	(5)
		Arc of Deforestation			Non-Forest
		Panel A: Contemporaneous Effect			
	All	All	Tropics	Non-Tropics	All
ΔKDD	0.00050	-0.00029	-0.00059	0.00007	0.00016***
	(0.00037)	(0.00049)	(0.00063)	(0.00039)	(0.00005)
Observations	48808	48497	20795	27684	186751
R-squared	0.191	0.454	0.480	0.400	0.294
		Panel B: Cumulative Effect			
Sum of ΔKDD	0.00592**	0.00753***	0.00707**	0.00845**	0.00129***
	(0.00268)	(0.00200)	(0.00232)	(0.00333)	(0.00029)
Observations	48808	48497	20795	27684	186751
R-squared	0.191	0.454	0.480	0.400	0.294
Grid-Cell Fixed Effects	Yes	Yes	Yes	Yes	Yes
Year Fixed Effects	Yes	No	No	No	No
Country-Year Fixed Effects	No	Yes	Yes	Yes	Yes

Notes: This Table reports estimates of the effect of killing degree days on deforestation, where the latter is measured using data from the European Space Agency land cover dataset (Zanaga et al., 2021) (compare to the main estimates in Table 1). Panel A reports estimates of equation (7). Panel B reports estimates of equation (8) for j between $-L = 0$ and $K = 4$, where "Sum of ΔKDD" corresponds to the sum of coefficients: $\beta_0 + \beta_1 + \beta_2 + \beta_3 + \beta_4$. The set of included fixed effects is listed at the bottom of each column and the sample is noted at the top. The Tropics are defined as all grid cells that fall between the Tropic of Cancer and the Tropic of Capricorn, and the Non-Tropics as the complement. The Arc of Deforestation is defined in Section 3.3 to identify the edge of the world's forests, and the Non-Forest denotes grid cells with less than 50% tree cover. Standard errors, reported in parentheses, are clustered by first-level administrative division (states within countries).

Table A.2: Alternative Definitions of the Arc of Deforestation

	(1) Forest 50%	(2) Forest 30%	(3) Forest 80%	(4) Pre-period	(5) Ever in Arc
	Panel A: In Arc of Deforestation				
Sum of Δ KDD	0.02331***	0.01516***	0.00942***	0.02313***	0.02298***
	(0.00538)	(0.00261)	(0.00244)	(0.00437)	(0.00401)
Observations	36779	65215	8594	42084	44044
R-squared	0.496	0.432	0.631	0.410	0.418
	Panel B: Not in Forest				
Sum of Δ KDD	0.00018	0.00006	0.00010	0.00004	0.00008
	(0.00021)	(0.00009)	(0.00040)	(0.00016)	(0.00017)
Observations	190763	153037	222664	184170	188692
R-squared	0.441	0.419	0.461	0.338	0.354
Grid-Cell Fixed Effects	Yes	Yes	Yes	Yes	Yes
Country-Year Fixed Effects	Yes	Yes	Yes	Yes	Yes

Notes: This table reports the effects of extreme temperature changes on deforestation using different definitions of the Arc of Deforestation. Each panel reports estimates of equation (8) for j between $-L = 0$ and $K = 4$, where "Sum of ΔKDD" corresponds to the sum of coefficients: $\beta_0 + \beta_1 + \beta_2 + \beta_3 + \beta_4$. Panel A includes all grid cells in the Arc of Deforestation and Panel B includes all grid cells outside the forest. Columns 1-3 define forested area as grid cells with 50%, 30%, and 80% forest cover respectively, and then define the Arc of Deforestation with respect to these forest definitions. In column 4, we fix the Arc of Deforestation at its pre-period level, and in column 5 we include a cell in the Arc of Deforestation if it is ever included in the Arc of Deforestation using the column 1 (baseline) definition. Standard errors, reported in parentheses, are clustered by first-level administrative division (states within countries).

Table A.3: Extreme Heat Causes Deforestation at Different Grid-Cell Levels

	(1)	(2)	(3)	(4)	(5)
		Arc of Deforestation			Non-Forest
	All	All	Tropics	Non-Tropics	All
			Panel A: 1 Degree Grid (Baseline)		
Sum of ΔKDD	0.02534***	0.02331***	0.02634***	0.01083**	0.00018
	(0.00496)	(0.00538)	(0.00653)	(0.00419)	(0.00021)
Observations	48875	48564	20826	27738	243756
R-squared	0.430	0.497	0.575	0.383	0.413
			Panel B: 5 Degree Grid		
Sum of ΔKDD	0.03257***	0.03114***	0.03247***	0.02739	-0.00036
	(0.00519)	(0.00779)	(0.00886)	(0.02504)	(0.00070)
Observations	2179	1958	1082	816	10,169
R-squared	0.761	0.882	0.888	0.757	0.708
Grid FE	Yes	Yes	Yes	Yes	Yes
Year FE	Yes	No	No	No	No
Country-Year FE	No	Yes	Yes	Yes	Yes

Notes: This table reports the effects of extreme temperature changes on deforestation at two different levels of geographic aggregation: 1=degree latitude-by-longitude grid cells in Panel A (baseline) and 5-degree latitude-by-longitude grid cells in Panel B. Both panels report estimates of equation (8) for j between $-L = 0$ and $K = 4$, where "Sum of ΔKDD" corresponds to the sum of coefficients: $\beta_0 + \beta_1 + \beta_2 + \beta_3 + \beta_4$. The set of included fixed effects is listed at the bottom of each column and the sample is noted at the top. The Tropics are defined as all grid cells that fall between the Tropic of Cancer and the Tropic of Capricorn, and the Non-Tropics as the complement. The Arc of Deforestation is defined in Section 3.3 to identify the edge of the world's forests, and the Non-Forest denotes grid cells with less than 50% tree cover. Standard errors, reported in parentheses, are clustered by first-level administrative division (states within countries).

Table A.4: Temperature Extremes Cause Deforestation: All Forested Area

	(1)	(2)	(3)	(4)
	Full Forest ($> 50\%$ Tree Cover)			
	All	All	Tropics	Non-Tropics
	Panel A: Contemporaneous Effect			
ΔKDD	0.00150**	0.00208***	0.00246***	0.00035
	(0.00061)	(0.00062)	(0.00075)	(0.00059)
Observations	55671	55360	26825	28535
R-squared	0.441	0.502	0.589	0.377
	Panel B: Cumulative Effects			
Sum of ΔKDD	0.02301***	0.02033***	0.02183***	0.01096***
	(0.00369)	(0.00405)	(0.00474)	(0.00419)
Observations	55671	55360	26825	28535
R-squared	0.441	0.502	0.589	0.377
Grid-Cell Fixed Effects	Yes	Yes	Yes	Yes
Year Fixed Effects	Yes	No	No	No
Country-Year Fixed Effects	No	Yes	Yes	Yes

Notes: This table reports the effects of extreme temperature changes on deforestation in the all of the world's forest (defined as grid cells with $> 50\%$ tree cover, in contrast to our baseline analysis which focuses on the Arc of Deforestation (see Table 1). Panel A reports estimates of equation (7). Panel B reports estimates of equation (8) for j between $-L = 0$ and $K = 4$, where "Sum of ΔKDD" corresponds to the sum of coefficients: $\beta_0 + \beta_1 + \beta_2 + \beta_3 + \beta_4$. The set of included fixed effects is listed at the bottom of each column and the sample is noted at the top. The Tropicsare defined as all grid cells that fall between the Tropic of Cancer and the Tropic of Capricorn, and the Non-Tropics as the complement. Standard errors, reported in parentheses, are clustered by first-level administrative division (states within countries).

Table A.5: Temperature Extremes Causes Deforestation: Place-Specific Linear Trends

	(1)	(2)	(3)	(4)	(5)
		Arc of Deforestation			Non-Forest
	All	All	Tropics	Non-Tropics	All
			Panel A: Contemporaneous Effect		
ΔKDD	0.00175***	0.00243***	0.00322***	0.00016	-0.00000
	(0.00065)	(0.00071)	(0.00080)	(0.00056)	(0.00002)
Observations	48875	48564	20826	27738	243756
R-squared	0.529	0.582	0.662	0.468	0.529
			Panel B: Cumulative Effect		
Sum of ΔKDD	0.02751***	0.02536***	0.02927***	0.00460	0.00021
	(0.00615)	(0.00616)	(0.00676)	(0.00383)	(0.00019)
Observations	48875	48564	20826	27738	243756
R-squared	0.529	0.582	0.662	0.468	0.529
Grid-Cell Fixed Effects	Yes	Yes	Yes	Yes	Yes
Grid-Cell Linear Trends	Yes	Yes	Yes	Yes	Yes
Year Fixed Effects	Yes	No	No	No	No
Country-Year Fixed Effects	No	Yes	Yes	Yes	Yes

Notes: This table reports the effects of extreme temperature changes on deforestation from regression models with place-specific linear trends: that is, for each grid cell i, a regressor of the form $\tau_i \cdot t$ (compare to the baseline in Table 1). Panel A reports estimates of equation (7) augmented with place-specific linear trends. Panel B reports estimates of equation (8) augmented with place-specific linear trends, for j between $-L = 0$ and $K = 4$, where "Sum of ΔKDD" corresponds to the sum of coefficients: $\beta_0 + \beta_1 + \beta_2 + \beta_3 + \beta_4$. The set of included fixed effects is listed at the bottom of each column and the sample is noted at the top. The Tropics are defined as all grid cells that fall between the Tropic of Cancer and the Tropic of Capricorn, and the Non-Tropics as the complement. The Arc of Deforestation is defined in Section 3.3 to identify the edge of the world's forests, and the Non-Forest denotes grid cells with less than 50% tree cover. Standard errors, reported in parentheses, are clustered by first-level administrative division (states within countries).

Table A.6: Extreme Heat Causes Deforestation Controlling for Upwind Deforestation

	(1)	(2)	(3)	(4)	(5)
		Arc of Deforestation			Non-Forest
	All	All	Tropics	Non-Tropics	All
			Panel A: Contemporaneous Effect		
Δ KDD	0.00240***	0.00310***	0.00414***	0.00036	-0.00000
	(0.00073)	(0.00081)	(0.00092)	(0.00062)	(0.00002)
Observations	48875	48564	20826	27738	243756
R-squared	0.446	0.508	0.588	0.392	0.418
			Panel B: Cumulative Effect		
Sum of ΔKDD	0.02220***	0.02120***	0.02459***	0.01031**	0.00010
	(0.00469)	(0.00529)	(0.00645)	(0.00398)	(0.00018)
Observations	48875	48564	20826	27738	243756
R-squared	0.446	0.508	0.588	0.392	0.418
Grid-Cell Fixed Effects	Yes	Yes	Yes	Yes	Yes
Year Fixed Effects	Yes	No	No	No	No
Country-Year Fixed Effects	No	Yes	Yes	Yes	Yes
Upwind Def. Control	Yes	Yes	Yes	Yes	Yes

Notes: This table reports the effects of extreme temperature changes on deforestation augmented with a control variable measuring upwind deforestation (see Appendix C.1). Panel A reports estimates of equation (7). Panel B reports estimates of equation (8) for j between $-L = 0$ and $K = 4$, where "Sum of ΔKDD" corresponds to the sum of coefficients: $\beta_0 + \beta_1 + \beta_2 + \beta_3 + \beta_4$. The set of included fixed effects is listed at the bottom of each column and the sample is noted at the top. The Tropics are defined as all grid cells that fall between the Tropic of Cancer and the Tropic of Capricorn, and the Non-Tropics as the complement. The Arc of Deforestation is defined in Section 3.3 to identify the edge of the world's forests, and the Non-Forest denotes grid cells with less than 50% tree cover. Standard errors, reported in parentheses, are clustered by first-level administrative division (states within countries).

B Dynamic Model

We extend the static model of Section 2 to incorporate multiple periods and adjustment costs in land clearing. Because of adjustment costs, deforestation responds gradually to changes in productivity, prices, and costs, as is consistent with our empirical results in Figures 2 and 7 of Section 4.

Set-up. Time is discrete and infinite, indexed by $t \in \mathbb{N}$. We focus on the problem of a single farmer in location i. This farmer chooses the stock of land used in each period, $x_{it} \in \mathbb{R}_+$. As in Section 2, we interpret all unused land as "forest," such that increases in land use correspond to deforestation. The farmer's per-period flow utility, as a function of the current and previous stock, is

$$\pi(x_{it}, x_{i,t-1}) = p_{it} a_{it} x_{it} - \frac{c_{it}}{2} x_{it}^2 - \frac{\gamma_{it}}{2}(x_{it} - x_{i,t-1})^2 \tag{17}$$

As in our baseline model, $p_{it} \in \mathbb{R}_+$ is the (shadow) price of agricultural output, $a_{it} \in \mathbb{R}_+$ is physical productivity, and $c_{it} \in \mathbb{R}_+$ is the time-varying opportunity cost of deploying agricultural land. The final term is new to the dynamic model, and it represents adjustment costs, scaled by parameter $\gamma_{it} \in \mathbb{R}_+$. This term captures the costs of deploying technology to clear the forest, including cutting trees, setting fires, and clearing the ground. The first difference of land use corresponds to deforestation: $d_{it} = x_{it} - x_{i,t-1}$. For simplicity, adjustment costs are symmetric for deforestation ($d_{it} > 0$) and afforestation ($d_{it} < 0$).

At time $t = 0$, the farmer takes as given an initial land use $x_{i,-1}$ and the sequence of parameters $(p_{it}, a_{it}, c_{it}, \gamma_{it})_{t=0}^{\infty}$. They choose a path of land use to maximize the present discounted value of profits:

$$\max_{(x_{it})_{t=0}^{\infty}} \left\{ \sum_{t=0}^{\infty} \delta^t \pi(x_{it}, x_{i,t-1}) \right\} \quad \text{given } x_{i,-1} \tag{18}$$

where $\delta \in (0, 1)$ is the discount factor.

Land-use Dynamics. Taking the first-order condition of equation (18) with respect to x_{it}, for any $t \geq 0$, yields the difference equation

$$p_{it} a_{it} - c_{it} x_{it} - \gamma_{it}(x_{it} - x_{i,t-1}) + \delta \gamma_{i,t+1}(x_{i,t+1} - x_{it}) = 0 \tag{19}$$

This expression nests the first-order condition of the static problem when $\gamma_{it} = 0$ for all t. Otherwise, the additional γ_{it} terms reflect adjustment costs: using more land today is "cheaper" if more land was used yesterday and if more land is planned to be used

tomorrow. Given the appropriate terminal condition, this difference equation can be solved forward to determine the optimal path of land use and deforestation.

To characterize these dynamics, we consider a stationary environment in which p_i, a_i, c_i, and γ_i are constant over time. Substituting in equation (19):

$$p_i a_i - c_i x_{it} - \gamma_i (x_{it} - x_{i,t-1}) + \delta \gamma_i (x_{i,t+1} - x_{it}) = 0 \tag{20}$$

In steady state, $x_{it} = x_i^*$ for all $t \geq 0$. Substituting and solving for x_i^*, we see that steady-state land use coincides with the prediction from the static model.

$$x_i^* = \frac{p_i a_i}{c_i} \tag{21}$$

Furthermore, we can rewrite equation (20) in terms of deviations $\hat{x}_{it} := x_{it} - x_i^*$ from the steady state:

$$\hat{x}_{i,t+1} = \left(\frac{c}{\delta \gamma} + \frac{1}{\delta} + 1 \right) \hat{x}_{it} - \frac{1}{\delta} \hat{x}_{i,t-1} \tag{22}$$

We guess and verify a solution in which $\hat{x}_{it} = \lambda^t (x_{i,-1} - x_i^*)$ for all $t \geq 0$. This solution describes geometric convergence to the steady state, with the speed of adjustment governed by λ and the magnitude of the transition determined by the initial deviation $x_{i,-1} - x_i^*$. Substituting the guess in the above expression for $t > 0$ and dividing by $\lambda^{t-1}(x_{i,-1} - x_i^*)$ gives:

$$\lambda^2 = \left(\frac{c}{\delta \gamma} + \frac{1}{\delta} + 1 \right) \lambda - \frac{1}{\delta} \tag{23}$$

This quadratic equation has one root that satisfies $\lambda \in (0, 1)$.

$$\lambda = \frac{c + (1+\delta)\gamma - \sqrt{(c + (1+\delta)\gamma)^2 - 4\delta\gamma^2}}{2\delta\gamma} \tag{24}$$

Hence, the dynamics of x_{it} are saddle-path stable.

The full dynamics of land use around the steady state are given by our solution

$$x_{it} = x_i^* + \lambda^t \left(x_{i,-1} - x_i^* \right) \quad \text{for } t \geq 0 \tag{25}$$

where λ is defined in equation (24). Deforestation $d_{ir} = x_{ir} - x_{i,r-1}$ is

$$d_{it} = \lambda^r (\lambda^{-1} - 1) \left(x_i^* - x_{i,-1} \right) \quad \text{for } t \geq 0 \tag{26}$$

Thus, the sign of deforestation depends on the sign of $x_i^* - x_{i,-1}$. If initial land use is

less than the steady state, then the farmer deforests in every period $t \geq 0$. Moreover, for $\lambda \in (0,1)$, λ^t converges to zero and $|d_{it}|$ decreases over time. The farmer deforests (or aforests) most at time 0 and less so at time $t > 0$ as land use transitions to the steady state.

Comparative Statics. The parameter γ, which controls adjustment costs, has no effect on the steady-state level of land use. It affects only the transition dynamics, as higher adjustment costs (higher γ) slow the transition to the steady state (higher λ):

$$\frac{\partial \lambda}{\partial \gamma} = \frac{\lambda}{\gamma\sqrt{(c+(1+\delta)\gamma)^2 - 4\delta\gamma^2}} > 0 \tag{27}$$

The parameter δ, which controls discounting, similarly affects only the transition path. More patience (higher δ) speeds the transition to the steady state (lower λ):

$$\frac{\partial \lambda}{\partial \delta} = -\lambda - \frac{1}{2\delta}\left(\frac{c+(1+\delta)\gamma}{\sqrt{(c+(1+\delta)\gamma)^2 - 4\delta\gamma^2}} - 1\right) < 0 \tag{28}$$

The parameters a_i and p_i affect the steady state, as seen in equation 21, but not the transition dynamics, as summarized by λ in equation 24. Their effect on the steady state is as in the main analysis: higher productivity or prices raise land use. The parameter c affects the steady state as in the static analysis, as higher costs lead to less land use. It also affects transition dynamics, as higher costs lead to slower transitions (higher λ):

$$\frac{\partial \lambda}{\partial c} = \frac{1}{2\delta\gamma}\left(\frac{c+(1+\delta)\gamma}{\sqrt{(c+(1+\delta)\gamma)^2 - 4\delta\gamma^2}} - 1\right) > 0 \tag{29}$$

Mapped back to our interpretation of parameters (see Section 2), the productivity and price channels affect the long-run level of forest cover and hence cumulative deforestation in response to a shock, while the cost channel affects both this cumulative level as well as the pace of deforestation. In particular, a shock that decreases the cost of deforestation both increases the steady-state level of land use and leads to an accelerated transition.

From Theory to Empirics. The dynamic event-study model of equation (8), i.e.,

$$\text{Deforestation}_{it} = \sum_{j=-L}^{K} \beta_j \Delta\text{KDD}_{i,t-j} + \gamma_i + \chi_{c(i),t} + \epsilon_{it} \tag{30}$$

can be used to determine the empirical analogue of a sudden and permanent jump in killing degree days. In particular, consider the case in which

$$\Delta \text{KDD}_{is} = \begin{cases} \Delta > 0 & \text{if } s = t \\ 0 & \text{otherwise} \end{cases} \tag{31}$$

The effect on deforestation according to the model of equation (8), holding fixed γ_i and $(\chi_{c(i),s}, \epsilon_{is})$ for all s, is

$$\text{Deforestation}_{is} = \begin{cases} \beta_{s-t}\Delta & \text{if } -L \leq s-t \leq K \\ 0 & \text{otherwise} \end{cases} \tag{32}$$

Thus, the time path of deforestation visually resembles the sequence of coefficients plotted in Figure 2, where the horizontal access increments from $t-4$ to $t+4$.

The experiment we consider in the model is an unanticipated, permanent change to parameters that increases steady-state land use. This corresponds to the transition dynamics of equation (26), where x_i^* is the new steady state and $x_{i,-1} < x_i^*$ is the original steady state. This pattern of gradual deforestation in response to the shock is qualitatively consistent with our empirical estimates.

C Data

C.1 Upwind Deforestation Exposure

We calculate upwind deforestation exposure following Araujo et al. (2023). In Table A.6, we present estimates of our main specification measuring the effects of temperature extremes on deforestation after controlling for this measure.

We measure wind patterns using the monthly wind fields produced as part of the ERA5 dataset (Muñoz Sabater et al., 2021) and deforestation, as in our main analysis, with the dataset of Hansen et al. (2013). Our objective is to measure, for every $1^\circ \times 1^\circ$ grid cell, the share of deforestation in upwind areas to which it is exposed.

We first compute wind direction θ (in degrees) and speed s (in meters per second) at each vertex of our dataset (i.e., each of the corners of the grid cells), indexed by v, in each

month, indexed by calendar month m and year t:

$$\theta_{v,m,t} = \big(\arctan 2(v10_{o(v),m,t}, u10_{o(v),m,t})\big) \bmod 360^\circ, \quad s_{o(v),m,t} = \sqrt{u10^2_{o(v),m,t} + v10^2_{o(v),m,t}} \tag{33}$$

where $o(v)$ denotes the origin grid cell; $\arctan 2$ denotes the two-argument arctangent (i.e., $\arctan 2(y, x)$ denotes the angle from the x-axis to the coordinate (x, y)); and $v10$ and $u10$ are the northern and eastern components of the 10-meter wind direction.

We compute exposure based on 24 hours of wind travel. The great-circle distance covered in this time is $L_{v,m,t} = s_{v,m,t} \times 24 \times 3600$, since speed is computed in meters per second. We project winds emanating from each vertex v at the angle $\theta_{v,m,t}$, and we denote the resulting line segment as $\ell_{v,m,t}$.

We next intersect each wind exposure segment $\ell_{v,m,t}$ with every grid cell polygon $c \in \mathcal{G}$ to obtain the set of intersected polygons. We let the indicator $I_{v,c,m,t} \in \{0, 1\}$ denote whether grid cell polygon $c \in \mathcal{G}$ intersects with the segment $\ell_{v,m,t}$.

We next calculate exposure. For origin cell o and target cell c, the fraction of vertices whose monthly trajectories reach c is

$$\omega_{o,c,m,t} \;=\; \frac{1}{4} \sum_{v \in \mathcal{V}_o} I_{v,c,m,t}. \tag{34}$$

where $\mathcal{V}_o$ is the set of four vertices of the origin cell. Then, summing over all 12 months per year and origin grid cells, we calculate exposure to deforestation using these weights:

$$E_{c,t} = \sum_m \sum_{o \in \mathcal{G}} \omega_{o,c,m,t} D_{o,t} \tag{35}$$

Finally we rescale within each year to obtain a unit-free index:

$$\tilde{E}_{c,t} \;=\; \frac{E_{c,t}}{\max\limits_{c' \in \mathcal{G}} E_{c',t}} \;\in\; [0, 1] \tag{36}$$

This is our final measure of upwind exposure.

C.2 Future Temperature Projections

We construct future temperature projections using an ensemble of global climate models from the Coupled Model Intercomparison Project Phase 6 (CMIP6). We use the following CMIP6 climate models in our analysis: CMCC-ESM2, EC-Earth3-Veg-LR, EC-Earth3, GFDL-CM4, GFDL-CM4_gr2, GFDL-ESM4, INM-CM4-8, INM-CM5-0, IPSL-CM6A-LR,

KACE-1-0-G, KIOST-ESM, MIROC6, MPI-ESM1-2-HR, MPI-ESM1-2-LR, and MRI-ESM2-0. These models span all major CMIP6 modeling centers and represent a broad range of structural assumptions regarding atmospheric physics, ocean dynamics, and land–atmosphere interactions. In our analysis, we assign each model an equal weight and compute the simple ensemble mean across all available models.